



**HAL**  
open science

## Mcl1 protein levels and Caspase-7 executioner protease control axial organizer cells survival

Elena Sena, Johnny Bou-Rouphael, Nathalie Rocques, Clémence Carron-Homo, Beatrice Claude Durand

► **To cite this version:**

Elena Sena, Johnny Bou-Rouphael, Nathalie Rocques, Clémence Carron-Homo, Beatrice Claude Durand. Mcl1 protein levels and Caspase-7 executioner protease control axial organizer cells survival. *Developmental Dynamics*, 2020, 249 (7), pp.847-866. 10.1002/dvdy.169 . hal-02562454

**HAL Id: hal-02562454**

**<https://hal.science/hal-02562454>**

Submitted on 24 Nov 2020

**HAL** is a multi-disciplinary open access archive for the deposit and dissemination of scientific research documents, whether they are published or not. The documents may come from teaching and research institutions in France or abroad, or from public or private research centers.

L'archive ouverte pluridisciplinaire **HAL**, est destinée au dépôt et à la diffusion de documents scientifiques de niveau recherche, publiés ou non, émanant des établissements d'enseignement et de recherche français ou étrangers, des laboratoires publics ou privés.

# Mcl1 protein levels and Caspase-7 executioner protease control axial organizer cells survival

Elena Sena<sup>1,2</sup>  | Johnny Bou-Rouphael<sup>3</sup> | Nathalie Rocques<sup>1,2</sup> | Clémence Carron-Homo<sup>3</sup> | Béatrice C. Durand<sup>1,2,3</sup> 

<sup>1</sup>Institut Curie, PSL Research University, Orsay, France

<sup>2</sup>Université Paris Sud, Orsay, France

<sup>3</sup>Sorbonne Université, CNRS UMR7622, IBPS Developmental Biology Laboratory, Paris, France

## Correspondence

Sorbonne Université, CNRS UMR7622, IBPS Developmental Biology Laboratory, Paris, France.

Email: [beatrice.durand@sorbonne-universite.fr](mailto:beatrice.durand@sorbonne-universite.fr)

## Present address

Nathalie Rocques, Ecole Polytechnique, Université Paris-Saclay, Palaiseau, France

## Funding information

Association pour la Recherche sur le Cancer, Grant/Award Number: DOC20170505923; Centre National de la Recherche Scientifique, Grant/Award Number: CNRS—UMR3347; Fondation Pierre Gilles de Gennes, Grant/Award Number: FPGG0039; Institut National de la Santé et de la Recherche Médicale, Grant/Award Number: INSERM—U1021; Ligue Nationale contre le Cancer Comité Ile de France, Grant/Award Number: RS19/75-52

## Abstract

**Background:** Organizing centers are groups of specialized cells that secrete morphogens, thereby influencing development of their neighboring territories. Apoptosis is a form of programmed cell death reported to limit the size of organizers. Little is known about the identity of intracellular signals driving organizer cell death. Here we investigated in *Xenopus* the role of both the anti-apoptotic protein Myeloid-cell-leukemia 1 (Mcl1) and the cysteine proteases Caspase-3 and Caspase-7 in formation of the axial organizing center—the notochord—that derives from the Spemann organizer, and participates in the induction and patterning of the neuroepithelium.

**Results:** We confirm a role for apoptosis in establishing the axial organizer in early neurula. We show that the expression pattern of *mcl1* is coherent with a role for this gene in early notochord development. Using loss of function approaches, we demonstrate that Mcl1 depletion decreases neuroepithelium width and increases notochord cells apoptosis, a process that relies on Caspase-7, and not on Caspase-3, activity. Our data provide evidence that Mcl1 protein levels physiologically control notochord cells' survival and that Caspase-7 is the executioner protease in this developmental process.

**Conclusions:** Our study reveals new functions for Mcl1 and Caspase-7 in formation of the axial signalling center.

## KEYWORDS

apoptosis, mcl1, neuroepithelium, organizer, xenopus

## 1 | INTRODUCTION

Apoptosis is a form of cell death characterized by a series of morphological changes in the dying cells such as fragmentation and condensation of the chromatin, as well as secretion of apoptotic factors, which induce the absorption of the apoptotic cell by macrophages<sup>1</sup> (reviewed in

Reference 2. In vertebrates, studies on apoptosis during embryonic development—also called early programmed cell death (PCD)—have largely focused on cell number regulation during organogenesis (reviewed in References 3, 4. However, apoptosis fulfills important roles during patterning of the neuroepithelium, which are not entirely deciphered (reviewed in References 4-8. Neural patterning is under the control of localized organizing centers that secrete morphogens, which influence development of organizers' neighboring territories (reviewed in

Elena Sena and Johnny Bou-Rouphael authors contributed equally to the work.

References 9-12. In amphibian, chicken, and mice, apoptosis has been reported to: limit the size, sculpt, and sometimes erase the organizer<sup>13-16</sup> (reviewed in Reference 4. Other studies performed in amphibians describe a role for the apoptotic machinery in primary neurogenesis.<sup>8,17</sup> Currently, the intracellular signals that influence cell survival at these early developmental stages remain unknown (reviewed in References 4, 6.

Extensive work in the nematode *Caenorhabditis elegans* (*C. elegans*), the fruit fly *Drosophila*, and vertebrates, including mammals, has led to a better understanding of the mechanisms driving cell death, revealing that apoptosis is implemented through the activation of a conserved molecular pathway (reviewed in References 3, 18-21. Cell death signals ultimately drive the activation of initiator Caspase-9 and effector Caspases, such as Caspase-3 (Casp3) and Caspase-7 (Casp7), which leads to self-activation of Caspases by proteolytic cleavage and irreversibly to cell death by triggering degradation of the DNA and other vital cell components (reviewed in References 22-24. Noteworthy both initiator and effector Caspases display nonapoptotic activities that participate in the terminal differentiation of specialized cells, specifically in rodent lens epithelial cells<sup>25</sup> and in human keratinocytes.<sup>26</sup> In *Drosophila*, maintaining Caspases in an activated state while preventing the execution of the apoptotic program can lead to the production, by « undead cells », of high levels of signaling molecules from the Wnt, Tgf- $\beta$ , and Sonic Hedgehog (Shh) families. Secretion, generated by Caspases activities, induces overgrowth in the neighboring tissues (reviewed in References 27, 28

Beside Caspases, the main components of the apoptotic cascade are the B-cell lymphoma 2 (Bcl2) family proteins. Bcl2 proteins include anti-apoptotic proteins such as Bcl2, Myeloid cell leukemia 1 (Mcl1), and Bcl2 like-1 (Bcl2l1); and also pro-apoptotic proteins including Bcl2 associated protein X (Bax), Bcl2 antagonist killer 1 (Bak), BH3 interacting domain death agonist (Bid) and *bcl2 like 11* (*bcl2l11*, also known as *bim*)<sup>29,30</sup> (reviewed in References 31, 32. Current knowledge explains that in most cells the ratio of pro- vs anti- apoptotic proteins of the Bcl2 family controls whether a cell lives or dies.<sup>33,34</sup> In *Xenopus laevis* (*X. laevis*) eggs, analysis of RNA expression levels of Bcl2 family members revealed the presence of the anti-apoptotic *bcl2*, *bcl2-like 10* (*bcl2l10*, also known as *bcl-b*), *bcl2-like 2* (*bcl2l2*, also known as *bcl-w*), *bcl-x<sub>i</sub>* (long isoform encoded by *bcl2l1*) and *mcl1* transcripts. In those eggs Bcl-W, Bcl-X<sub>L</sub>, and Mcl1 efficiently inhibit apoptosis, with Mcl1 appearing to play key role in modulating the survival balance between pro- and anti-apoptotic activities.<sup>30</sup>

During amphibians' late gastrulation and early neurulation, apoptotic nuclei are reproducibly observed in the axial mesoderm—notochord and prechordal plate—, which secretes Bone morphogenetic protein (Bmp) inhibitors, including Chordin, and in the neural plate's midline (floor plate), which secretes Shh.<sup>16,35,36</sup> In *X. laevis* embryos overexpression of *Xenopus bcl-x<sub>i</sub>* or human *bcl2*, and the use of pan-Caspases inhibitors, like Z-DEVD-fmk and z-VAD, decreases cell death at late gastrula and early neurula stages.<sup>16,35-39</sup> Inhibition of apoptosis increases both the size of the neural plate, and the number of Chordin- and Shh-secreting cells. Therefore, in this context, it has been suggested that the apoptotic program participates in establishment of the axial organizer, and indirectly regulates formation of Bmp and Shh activities gradients.<sup>16,36</sup> Other studies, performed in amphibian, suggest a role for the apoptotic process in early neuroepithelial differentiation.<sup>8,17</sup> However, at this date, neither it is fully deciphered what are the functions of apoptosis, nor which endogenous apoptotic machinery factors—Bcl2-protein family members, and/or Caspases—contribute to the initiation and the induction of apoptosis within the emerging neural plate.

During nematode embryogenesis, the regulation of apoptosis is primarily regulated by transcriptional control of the cell-death execution machinery (reviewed in Reference 40. In vertebrates, a few homeodomain-containing proteins have been demonstrated to regulate apoptosis. Whether they do so by directly or indirectly modulating pro- or anti- apoptotic genes at the transcriptional level has not been addressed (reviewed in Reference 6. Investigation of Bar-class HD (Barh) transcription factors—BarH1 and BarH2—activities in nematode, *Xenopus* and mice revealed roles for these transcription factors in the developmental control of cell death<sup>16,41-45</sup> (reviewed in Reference 6. In *Xenopus*, *barH-like 2* (*barhl2*) depletion increases the number of axial organizer cells, whereas its overexpression increases apoptosis in the midline axial organizer between stage 10 and stage 14.<sup>16,46</sup> Whether Barhl2 affects the decision of axial organizer cells to die by transcriptional regulation of pro- or anti- apoptotic genes is unknown.

In this study we confirm that the apoptotic machinery participates to axial organizer development, and contributes indirectly to neural plate patterning. Both *mcl1* expression pattern and analysis of morpholino-mediated depletion of Mcl1 argue for a major contribution of Mcl1 in notochord cells survival. A form of Mcl1 mutated at its putative Glycogen synthase kinase 3- $\beta$  (Gsk3- $\beta$ ) phosphorylation site, which normally targets Mcl1 for degradation, displays an increased efficiency as an anti-apoptotic factor within the axial organizer cells. Moreover, Mcl1 depletion phenotype is mimicked

by overexpression of the pro-apoptotic factors Bax and Bak which both interact with Mcl1. Bax and Bak overexpression phenotypes are both rescued by

overexpression of Mcl1. Therefore, axial organizer cells' survival is physiologically controlled by Mcl1 protein levels. Whereas depletion of Casp3 activity neither alters

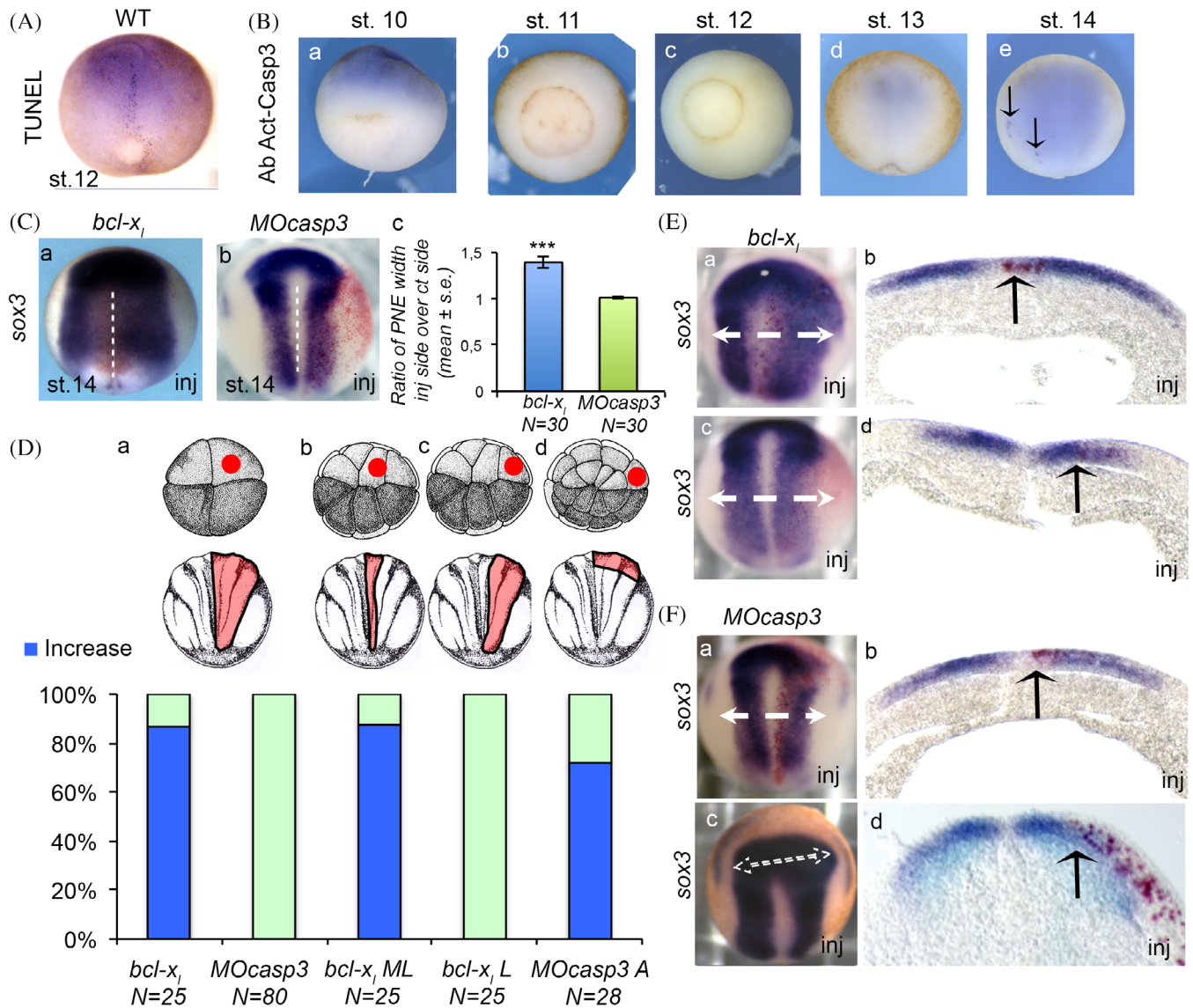


**FIGURE 1** Endogenous apoptosis contributes to axial organizer formation independently of Caspase3 activity. A, TUNEL-staining reveals apoptosis in the axial midline. Representative TUNEL-stained wild type (wt) stage (st.) 12 *Xenopus* embryos. B, Activated Caspase-3 (Act-Casp3) is not detected before stage 14 in *Xenopus* embryos. Representative immuno-staining against Act-Casp3 performed on st. 10 to st. 14 embryos. Act-Casp3 positive nuclei are shown with black arrows; st. 10 to 12 ventral view dorsal up; st. 13 and 14 dorsal view anterior up. C to F, Endogenous apoptosis affects establishment of the posterior neural plate via its activity on axial organizer signaling independently of Casp3. C, *Xenopus* embryos were injected into one dorsal blastomere at the four-cell stage with mRNA encoding (a) *X. laevis* *bcl-xl* or (b) *MOcasp3* together with a tracer (red) and analyzed by ISH with *sox3*. Representative st. 14 embryos are shown. (c) Quantification graph of (a,b). D, *Xenopus* embryos were injected into one dorsal blastomere at the four- (a), sixteen- (b,c) or thirty-two- (d) cells stage with mRNA encoding *X. laevis* *bcl-xl* or *MOcasp3* together with a tracer (red) and analyzed by ISH with *sox3*. The site of injection (red dot), and the corresponding st. 14 targeted territory (red area) are represented. The graph indicates the % of embryos exhibiting the (ac) posterior, or (d) anterior, neural plate enlargement phenotype (blue). ML: medio-lateral; L: lateral; A: anterior neural plate. E,F, *Bcl-XL* acts on the axial organizer cells. Embryos were injected either in the axial organizer (notochord and floor plate) or in lateral ectoderm with (E) *bcl-xl* or, F, *MOcasp3*. Representative embryos are shown dorsal view, anterior up, except (Fc) shown dorsal-anterior view. Representative transverse sections (50  $\mu$ m) are shown at the antero-posterior axis positions indicated with a white-dashed arrow (Eb,d; Fb,d). The black arrow indicates the limits of the injected territory. PNE: posterior neuroepithelium. Inj: injected side. White dashed lines indicate the midline. Relative normalized expression is indicated as means  $\pm$  SE (s.e.) \*\*\*P < .001

notochord nor neural plate development, morpholino-mediated Casp7 depletion both prevents embryos' apoptosis induced by Mcl1 depletion, and compensates for Mcl1 knockdown phenotype in the axial organizer. Finally, Barhl2 depletion does not affect RNA levels of most anti- or pro-apoptotic proteins, including those of *mcl1*. We conclude that in neurula embryos a decrease in Mcl1 protein levels physiologically triggers axial organizer cell death driven by Caspase-7 activation.

## 2 | RESULTS

### 2.1 | Endogenous apoptosis contributes to axial organizer formation through a pathway independent of Casp3

Apoptosis can be characterized by either DNA fragmentation, which is detected via Terminal deoxynucleotidyl transferase dUTP Nick End Labelling (TUNEL) staining, and/or via the presence of an activated form of Casp3 (Act-Casp3).<sup>47,48</sup> TUNEL analysis performed in *X. laevis* embryos between blastula and early neurula stages shows TUNEL positive nuclei around the blastopore and in the midline of the dorsal ectoderm and mesoderm.<sup>16,35,36</sup> We confirmed these observations performing TUNEL staining at stage 12 (Figure 1A) (this study and References 16, 36). We also performed immuno-staining against Act-Casp3 on stage 10 to stage 14 *X. laevis* embryos (Figure 1B). Surprisingly, we only detected a small number of cells expressing Act-Casp3 with none of them present in the midline (Figure 1Be).

We asked whether interference with developmental apoptosis, either by overexpression of the anti-apoptotic protein Bcl-X<sub>L</sub>, or depletion of the pro-apoptotic enzyme Casp3, affected development of the neural plate similarly. We overexpressed *X. laevis* *bcl-x<sub>L</sub>* or used previously validated MO specific of Casp3 (*MOcasp3*),<sup>49</sup> and followed establishment of the neural plate using the early marker of neural commitment *sry-box 3* (*sox3*) by whole mount in situ hybridization (ISH) (Figure 1C). We observed that *bcl-x<sub>L</sub>* overexpression generates a widening of the neuroepithelium whereas *MOcasp3* does not (Figure 1C).

To validate that the enlargement of the neuroepithelium was due to Bcl-X<sub>L</sub> activity within the axial organizer we injected *bcl-x<sub>L</sub>* mRNA either in the dorsal mesoderm (prechordal plate and notochord) and axial ectoderm (floor plate) (Figure 1Db,Ea,b), or in medio-lateral ectodermal cells (Figure 1Dc,Ec,d). We observed that Bcl-X<sub>L</sub> overexpression, either in the entire neural plate or in the midline cells, generated an increase in *sox3* staining (Figure 1Da,b,Ea,b). In contrast, injection of *bcl-x<sub>L</sub>* in the medio-lateral neuroectodermal cells had

no effect on the size of the neuroepithelium (Figure 1Dc, Ec,d). When *MOcasp3* was targeted in the anterior neural plate, we observed an enlargement of the anterior neuroepithelium (Figure 1Dd,Fc,d), which can be explained by Casp3 function in patterning the anterior neural plate independently of its role in apoptosis.<sup>49</sup>

In conclusion, the increase in the neural plate size driven by Bcl-X<sub>L</sub> overexpression is an indirect consequence of apoptosis inhibition in axial organizer cells. At these developmental stages Casp3 activity is not strictly required in the axial midline.

### 2.2 | *mcl1* expression pattern indicates a possible role for this anti-apoptotic protein in axial organizer development

We next aimed to identify which apoptotic factors were involved in mediating axial organizer cell survival. Using Real Time quantitative PCR (RT-qPCR) on the dissected dorsal and ventral ectoderm of stage 13.5 *Xenopus* embryos, we investigated the presence of RNA encoding for pro- and anti-apoptotic members and measured the ratio of RNA transcripts enriched in the dorsal, relative to the ventral, ectoderm (Figure 2A). The genes studied were members of the Bcl2 family, which include the pro-apoptotic genes *bax*, *bak*, *bid*, and *bim* (*bcl2l11*), the genes encoding caspases (*casp9*, *casp3*, and *casp7*), and anti-apoptotic genes *bcl2l10* (*bcl-b*), *bcl2l2* (*bcl-w*), *bcl2l1* (*bcl-x<sub>L</sub>*), and *mcl1*. In agreement with databases,<sup>50,51</sup> we detected very low levels of *bax*, *bak*, *bid*, *bim*, and *bcl2l2*, and an increase neuroepithelial presence of transcripts encoding *casp9*, *casp3*, *casp7*, *bcl2l10*, *bcl-x<sub>L</sub>*, and *mcl1* (Figure 2A).

Both Bcl-x<sub>L</sub> and Mcl1 exhibit strong anti-apoptotic activities in *Xenopus* eggs.<sup>30</sup> In both *Xenopus tropicalis* (*X. tropicalis*) and rodents, the levels of *mcl1* transcripts have been reported to increase when maternal mRNA pools wane and embryonic gene expression starts (<sup>50</sup> reviewed in Reference 32). We next analyzed the expression pattern of *mcl1* and *bcl-x<sub>L</sub>* in *X. laevis* embryos at late gastrula, early neurula stages. Using ISH we observed that *mcl1* mRNA is weakly detected at stage 11; but between stage 13 and stage 20, *mcl1* transcripts are present within the neuroepithelium (Figure 2B). Between stage 13 and stage 16, *mcl1* transcripts are present in the anterior neuroectoderm, in two stripes along the forming axial organizer (Figure 2Bc,d), which appear on transverse section to be in the mesoderm and the neuroectoderm (Figure 2Bg). *mcl1* transcripts are also present at the border between the neuroectoderm and the ectoderm (Figure 2Bc). At stage 20, *mcl1* expression is detected within the future neural tube, specifically in the eye primordium. At the same

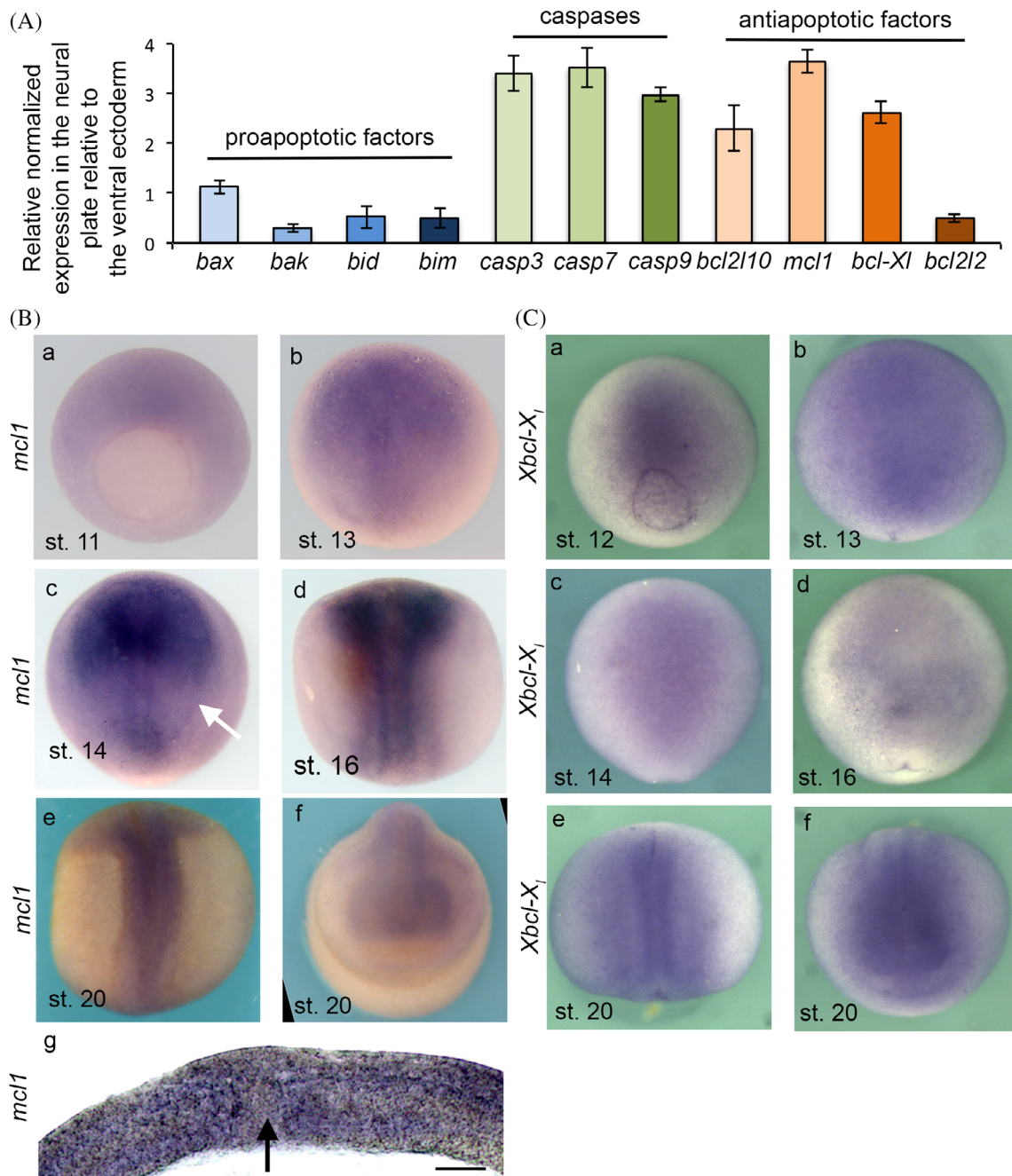


**FIGURE 2** *mcl1* expression pattern suggests a role for this protein in axial organizer development. A, RTqPCR analysis of apoptotic cascade mRNA in *Xenopus* early neurula. Analysis performed on RNA extracted from dissected neural plates, and ventral ectoderms ( $N = 15$ ) of *X. laevis* embryos at stage (st.) 14 for proapoptotic factors - *bak*, *bad*, *bid*, *bim*, including caspases (*casp*)—*casp3*, *casp7*, and *casp9* and antiapoptotic factors - *bcl2l10*, *mcl1*, *bcl-xl*, and *bcl2l2*. Expression is normalized relative to *ef1 $\alpha$* . Relative normalized expression is indicated as means  $\pm$  SE. B, *mcl1* expression pattern. ISH using a probe for *mcl1* from st. 11 to st. 20 embryos; (a) ventral view, dorsal up, (b–e) dorsal view anterior up, (f) anterior view dorsal up. (g) Transverse section of (c) in the posterior part of the embryo. The scale bar stands for 200  $\mu$ m. The white arrow indicates the border between the ectoderm and the neuroectoderm. The black arrow indicates the notochord. C, *bcl-xl* expression pattern in *X. laevis* gastrula and neurula. ISH using a probe for the anti-apoptotic gene *bcl-xl* from st. 12 to st. 20. Embryos are shown dorsal side up

developmental stages, we observed very low levels of expression of *bcl-xl* between stage 12 and stage 16 (Figure 2C). Our results are in agreement with *X. laevis* and

*X. tropicalis* data-bases reporting level of *mcl1* transcripts at stage 13 that are higher than any of the other *bcl2* anti-apoptotic proteins transcripts.<sup>50,51</sup>

Therefore, *mcl1* expression pattern is consistent with an early activity for this anti-apoptotic gene in axial organizer survival.

### 2.3 | Depletion of Mcl1 activity influences neuroepithelium development

We focused our study on the Mcl1 role during early neurulation, and asked whether depletion of Mcl1 activity influenced axial organizer size and neural plate formation. To inhibit Mcl1 activity we designed, in its 5' untranslated region, two antisense morpholinos (*MOmcl1-1* and *MOmcl1-2*) together with a control morpholino (*MOmcl1-ct*) and generated constructs coding for two tagged versions of Mcl1: Flag-Mcl1 and Mcl1-Myc. Whereas *MOmcl1-1* and *MOmcl1-2* bind *mcl1-myc* mRNA, they do not bind *flag-mcl1* mRNA. At stage 14, we observed a dose-dependent decrease in the width of the *sox3* expression domain in embryos injected with

either *MOmcl1-1*, or *MOmcl1-2*, but not on embryos injected with *MOmcl1-ct* (Figure 3A,B). The effect was observed along the entire anterior-posterior (AP) axis and was dose-dependent.

Specific antibodies against *Xenopus* Mcl1 are not available. To establish the specificity of the MO effect, we tested the ability of both MOs to inhibit translation of *mcl1-myc* mRNA. Western Blot (WB) analysis of stage 13 *Xenopus* protein extracts revealed that both *MOmcl1-1* and *MOmcl1-2* inhibited the translation of *mcl1-myc* while *MOmcl1-ct* did not (Figure 3C). Results were similar with *MOmcl1-1* and *MOmcl1-2*, however, *MOmcl1-2* generated stronger developmental disruptions. We therefore used *MOmcl1-1*, referred to as *MOmcl1*, for further experiments. We tested *MOmcl1* as a specific inhibitor of endogenous Mcl1 activity by co-injecting *MOmcl1* with *flag-mcl1* mRNA, which is not recognized by *MOmcl1* (Figure 3D,E). We first validated that RNA encoded by *flag-mcl1* is expressed in stage 13 *Xenopus*

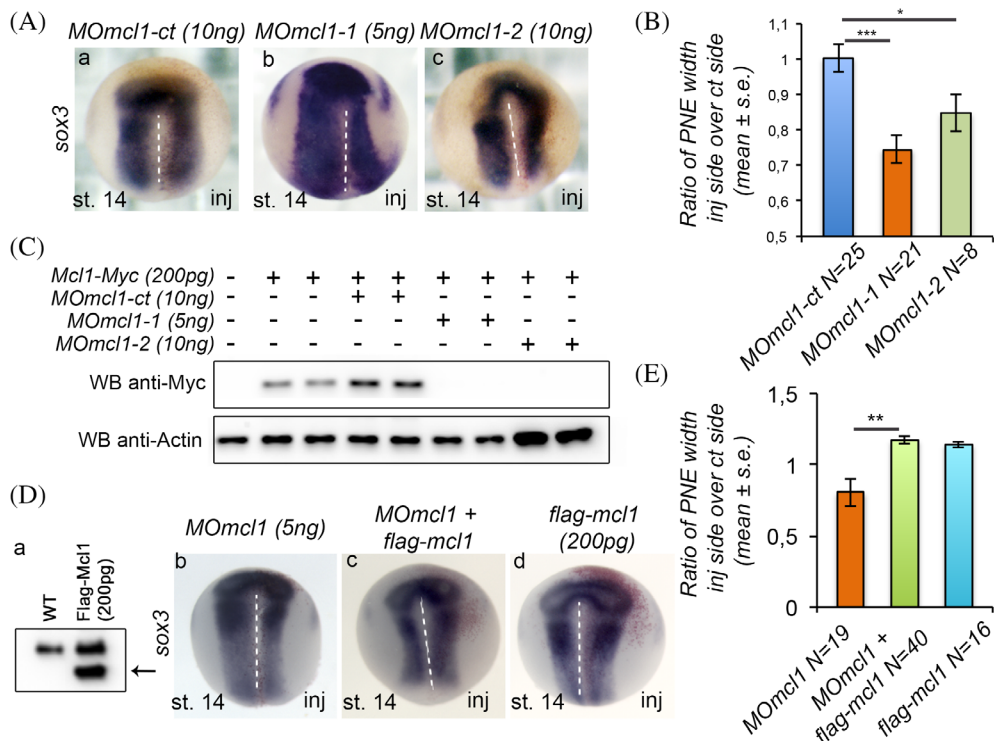


**FIGURE 3** Mcl1 depletion decreases the neuroepithelium size. A, Mcl1 MOs decrease the posterior neural plate width. ISH for *sox3*. Representative stage (st.) 14 embryos injected (inj) with (a) *MOmcl1-ct* (N = 25); (b) *MOmcl1-1* (N = 21); or (c) *MOmcl1-2* (N = 8). B, Quantification of A. C, *MOmcl1* blocks *mcl1* translation. Western Blot on st.13 *Xenopus* extracts using antibody against Myc-tag. Actin is used as a loading control. D, Flag-Mcl1 rescues the MO-mediated depletion of Mcl1. RNA encoding flag-Mcl1 or *MOmcl1-1* were injected in embryos either alone or together with a tracer (red) as indicated. (a) Western Blot using antiFlag antibody on st.13 *Xenopus* protein extracts injected with RNA encoding flag-mcl1 (200 pg). The black arrow indicates the band corresponding to the flag epitope of 33Kd. (b-d) ISH for *sox3*. Representative st.14 embryos are shown injected with (b) *MOmcl1-1* (N = 10), (c) *MOmcl1-1* and *flag-mcl1* (N = 40) or (d) *flagmcl1* alone (N = 16) at the indicated doses. E, Quantification of D. PNE: posterior neuroepithelium. White dashed line indicates the midline. Relative normalized expression is indicated as means ± SE. \* $P < .05$ , \*\* $P < .01$ , \*\*\* $P < .001$

protein extracts (Figure 3Da) and observed that Flag-Mcl1 significantly compensates for the decrease in neuroepithelium width induced by depletion of endogenous *mcl1* (Figure 3Db-d,E).

Together these results provide strong evidence that *MOmcl1* specifically inhibits endogenous Mcl1 activity, and that Mcl1 physiologically participates in neural plate induction.

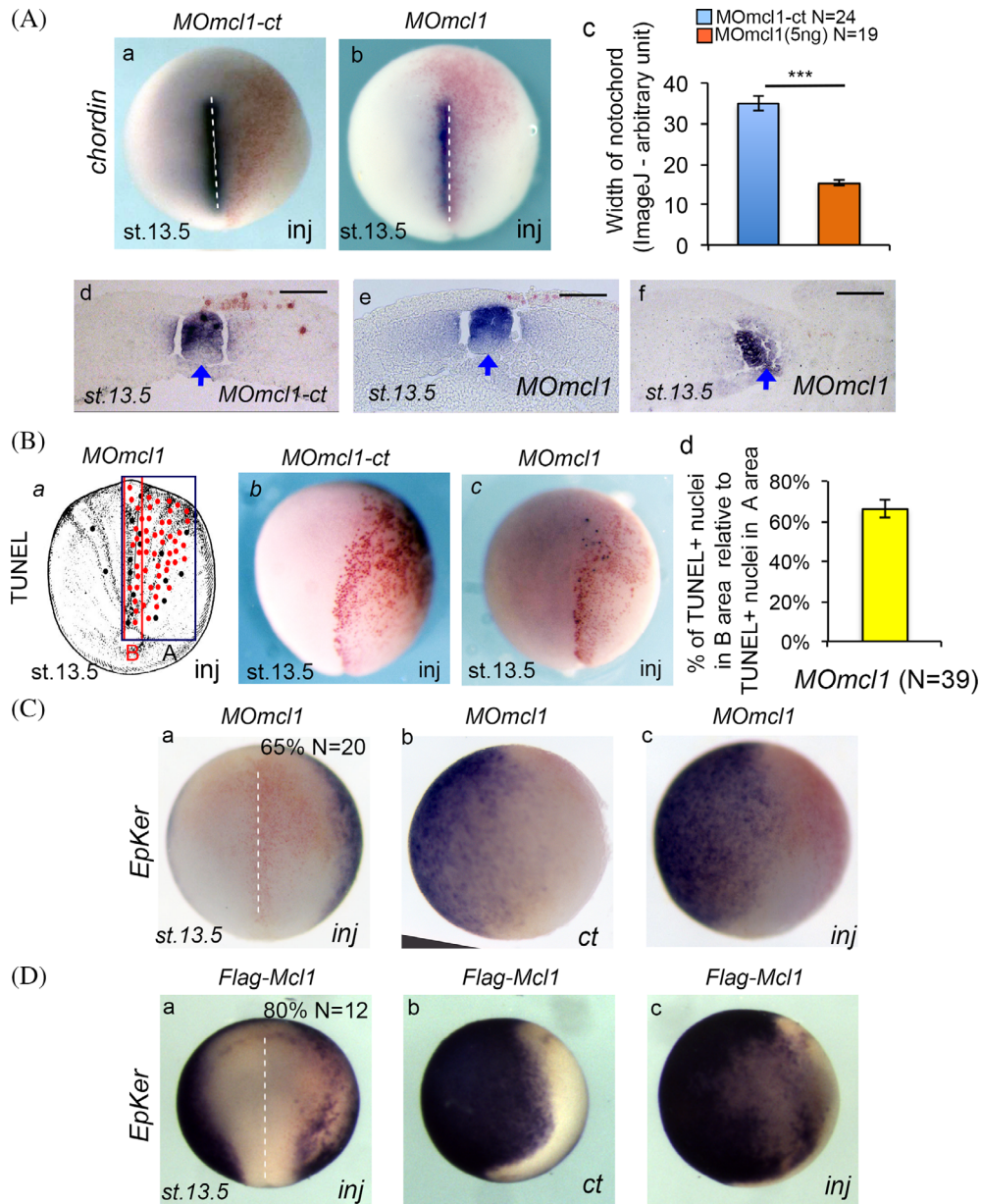


**FIGURE 4** Mcl1 depletion specifically affects the survival of notochord cells. A, Depletion of Mcl1 affects notochord development. ISH of stage (st.) 13.5 embryos using probes against chordin (a,b). Embryos injected (inj) with (a) *MOmcl1-ct* (N = 24); or (b) *MOmcl1* (N = 19); (c) Quantification graph showing notochord width comparison in embryos injected with *MOmcl1-ct* or *MOmcl1*. (d-f) Histological vibratome sections of respectively (d) *MOmcl1-ct* and (e,f) *MOmcl1*. Blue arrow indicates the notochord. Scale bar stands for 200  $\mu\text{m}$ . B, Quantification of midline apoptosis induced by Mcl1 depletion. TUNEL staining was performed at st.13.5. (a) Schematic representation of TUNEL quantification: red dots represent injected cells; black dots represent TUNEL positive cells. All apoptotic cells were counted in A the black rectangle considered the total injected area, and B the red rectangle considered the midline area. (b, c) Representative TUNEL staining on stage 13.5 embryos injected with (b) *MOmcl1-ct*; or (c) *MOmcl1* (N = 39). (d) Quantification of B. C,D, The decrease in neural plate width upon depletion of Mcl1 is mirrored by the increase in ectoderm territory. ISH against epidermal keratin (EpKer). Representative stage 13.5 embryo injected with C *MOmcl1-1*; D, *flag-mcl1*; (a) dorsal view anterior up; (b) View of the noninjected side: lateral view, anterior up, dorsal side right; (c) View of the injected side: lateral view, anterior up, dorsal side right. N represents the number of injected embryos. White dashed line indicates midline. Relative normalized expression is indicated as means  $\pm$  SE. \*\*\* $P < .001$

## 2.4 | Depletion of Mcl1 generates a loss of axial organizer cells and activity

*mcl1* transcripts are mostly detected along the axial midline in a territory bordering the axial organizer. We asked whether changes in the neural plate size caused by depletion of endogenous Mcl1 were generated by a decrease in notochord cell numbers and its subsequent decrease in neural induction activity, or due to an unspecific increase in neuroepithelial cells' death.

First, development of the notochord was assessed in Mcl1 depleted embryos at stage 13.5 using the dorsal mesoderm marker *chordin*. We observed a decrease in the size of *chordin*-expressing structure on the injected side of *MOmcl1* injected neurula embryos (Figure 4Aa-c). Transverse sectioning of *MOmcl1* injected embryos confirmed a diminution of the notochord size on the injected side (Figure 4Ad-f).

We next evaluated the Mcl1 depletion impact on notochord cells' death, vs neuro-epithelial cells' death. *MOmcl1*, or *MOmcl1-ct*, were injected into one dorsal blastomere at the 4-cell stage and TUNEL staining was performed at stage 13.5. We counted the number of apoptotic nuclei in the injected area (Figure 4Ba, zone A), and in the midline area (Figure 4Ba, zone B). Injection of *MOmcl1-ct* did not significantly increase the number of apoptotic nuclei in the dorsal part of the embryo (Figure 4Bb). In contrast, *MOmcl1* injection generated embryos displaying numerous apoptotic nuclei in their dorsal part (Figure 4Bc). Whereas the midline area corresponds to one quarter of the total area, in the Mcl1-depleted embryos,  $66 \pm 4\%$  of apoptotic nuclei were present within this midline domain (Figure 4Bd).

We reasoned that if the notochord was the structure preferentially affected by change in Mcl1 levels, a change in the neural plate size should be mirrored by a change in the ectoderm territory. We first followed formation of the epidermal territory in Mcl1 depleted neurula using *epidermal keratin* (*EpKer*) as a marker of the dorsal non-neural ectoderm. We observed an increase in *EpKer* expression on the *MOmcl1* injected side compared to the noninjected side (Figure 4C). In contrast, when *flag-mcl1* mRNA was injected we observed a decrease in *EpKer* expression on the injected side compared to the non-injected side (Figure 4D).

We conclude for a physiological role of Mcl1 in the survival of axial organizer cells.

## 2.5 | Depletion of the executioner Casp7 compensates for Mcl1 depletion

Casp3 and Casp7 are key mediators of mitochondrial apoptosis and are functionally redundant within the cell

death machinery<sup>52,53</sup> (reviewed in Reference 24. Our data indicate that Casp3 activity is dispensable for axial organizer formation. In agreement with our observations (Figure 2A), in both *X. tropicalis* and *X. laevis* a peak of *casp7* transcripts is detected between stage 5 and stage 15.<sup>50,51</sup> We asked whether, within the developing axial organizer, Casp7 physiologically acts as an executioner enzyme. We designed a splice modifying *casp7* specific morpholino (*MOcasp7*) that targets the acceptor site of Intron3—Exon4 of *casp7* mRNA (Figure 5Aa). Exon4 encodes both part of the substrate pocket, and the active site of Casp7 enzyme. Therefore, *MOcasp7* should induce the mis-splicing of *casp7* mRNA, and subsequently knockdown of Casp7 protease activity.

We first confirmed that *MOcasp7* injection in *Xenopus* embryos induced mis-splicing of the *casp7* mRNA (Figure 5Ab). At stage 14, embryos injected with *MOcasp7* display a dose-dependent increase in the width of the *sox3* expression domain, a phenotype not observed in embryos injected with *MOct* (Figure 5Bab,C). We next tested whether *MOcasp7* specifically inhibited Casp7 endogenous activity through co-injection of *MOcasp7* with human *casp7* (*hcasp7*) mRNA, which is not recognized by *MOcasp7*. At stage 14, overexpression of *hcasp7* significantly compensates the increase in neuroepithelium width induced by depletion of endogenous Casp7 (Figure 5Bb-d,C). These data provide strong evidence that *MOcasp7* inhibits endogenous Casp7 activity and suggest a role for Casp7 in the survival of axial organizer cells.

We next investigated whether Casp7 depletion would prevent apoptosis induced by Mcl1 depletion. *MOmcl1* injection at the lowest dose induces the death of about 60% of the total number of embryos, whereas coinjection of *MOcasp7* with *MOmcl1* significantly reduces the percentage of dead embryos (Figure 5D). We further asked whether Casp7 depletion compensates for Mcl1 loss of notochord activity. The impact of Casp7 on Mcl1 depletion phenotype was analyzed using *sox3*. As previously described, depletion of Mcl1 activity generated a diminution of the *sox3* expression territory (Figure 5Ea), whereas *MOcasp7* injected embryos exhibit a widening of the neural plate (Figure 5Bb, Ec). The co-injection of *MOmcl1* with *MOcasp7* fully rescues the neuroepithelium size defect (Figure 5Eb, F).

Therefore Casp7 is the executioner Caspase in the axial organizer cells death induced by *mcl1* depletion.

## 2.6 | Mcl1 protein levels are regulated within the axial organizer

In most cells the balance between the ratio of pro- vs anti-apoptotic proteins of the Bcl2 family decides

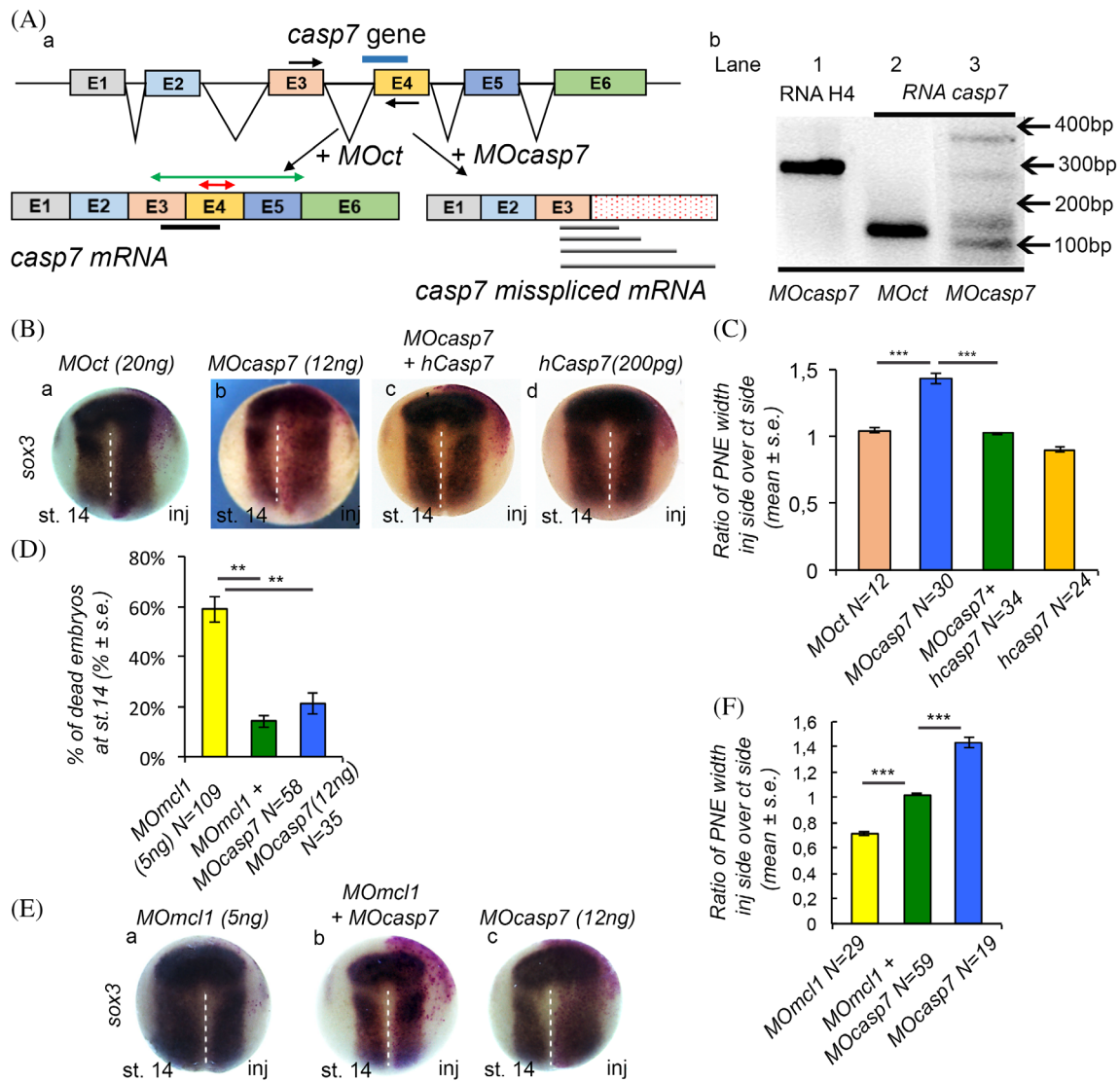


**FIGURE 5** Depletion of caspase-7 compensates for Mcl1 depletion. A, (a) Schematic representation showing the genomic organization of the caspase-7 gene (*casp7*) in *X. laevis*. The region targeted by the spliceblocking MO *casp7* (MOcasp7) is shown (blue line). The two black arrows indicate the location of the two primers used to amplify exon3 (E3) and exon4 (E4) sequences in the RT-PCR analysis (b). The substrate pocket (green double end arrow) and the active site (red double end arrow) are shown. (b) MOcasp7 efficacy was validated by RT-PCR using primers as indicated in (a). Total RNA was isolated from stage (st.) 14 MOcasp7 or control MO (MOct)- injected embryos and analyzed using E3-E4 *casp7* primers (a). Misspliced *casp7* mRNA forms are observed in MOcasp7 injected embryos compared to the normally spliced *casp7* mRNA detected in the MOct- injected embryos (Lanes 2 and 3). Histone H4 is used as an internal control and normally spliced in MOcasp7 injected embryos (Lane 1). B, Depletion of Casp7 increases neuroepithelium width. ISH of st. 14 embryos using probes against *sox3* (a-d). Embryos injected with (a) MOct (N = 12); (b) MOcasp7 (N = 30); (c) MOcasp7 together with human *casp7* (*hcasp7*) (N = 34) and (d) *hcasp7* (N = 24) at the indicated doses are shown dorsal view anterior up. C, Quantification of B. (D-F) Casp7 depletion rescues Mcl1 depletion apoptotic phenotypes. D, Percentage of dead embryos at st. 14 was calculated on MOmcl1 (N = 109), MOmcl1 together with MOcasp7 (N = 58), and MOcasp7 (N = 35) injected embryos. E, ISH using probes against *sox3* on embryos injected with (a) MOmcl1 (N = 29); (b) MOcasp7 and MOmcl1 (N = 59), or (c) MOcasp7 (N = 19). Representative embryos at st. 14 are shown dorsal view anterior up. F, Quantification of E. PNE stands for posterior neuroepithelium. The dashed white line indicates the midline. N represents the number of embryos. Relative normalized expression is indicated as means  $\pm$  SE. \*\**P* < .01, \*\*\**P* < .001

whether a cell lives or dies.<sup>33,34</sup> Compared with *bcl-x<sub>L</sub>*, *flag-mcl1* overexpression was poorly efficient in preventing the loss of notochord cells (Figure 3E). We asked whether Mcl1 protein levels could be physiologically controlled in axial organizer cells, and whether

Mcl1 presence in the notochord could be compensated for by overexpression of two pro-apoptotic factors known to bind and inhibit Mcl1 anti-apoptotic activity, human *bak*<sup>54</sup> and *Xenopus bak*<sup>55</sup> (reviewed in Reference 56).

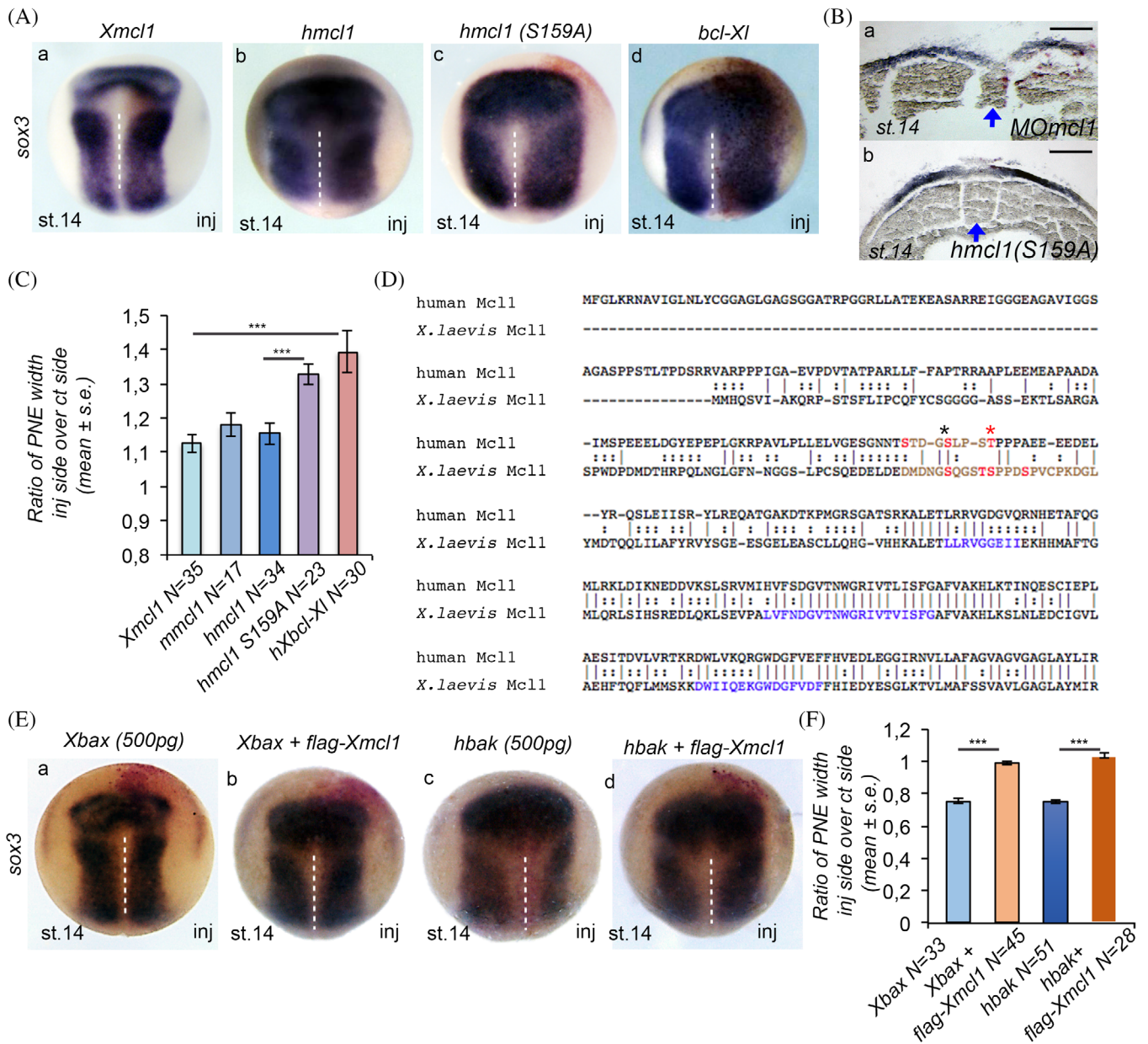


**FIGURE 6** A form of Mcl1 that cannot be phosphorylated by Gsk3 $\beta$  increases the neural plate size with a higher efficiency and compensates the overexpression of the pro-apoptotic proteins Xbax and hBak. A, ISH on stage (st.) 14 embryos using probes against *sox3* on embryos injected with (a) *Xenopus mcl1-myc (xmcl1)*, (b) human *mcl1 (hmcl1)*, (c) *hmcl1S159A* or (d) *Xenopus bcl-xl (bcl-xl)*. B, Histological sections of MOM*mcl1*- (a) and *hmcl1S159A*- (b) injected embryos at stage 14 following ISH using *sox3* probe and LacZ as a tracer. Blue arrow indicates the notochord. Scale bar stands for 200  $\mu\text{m}$ . C, Quantification of A with addition of mouse *mcl1 (mmcl1)* mRNA injected embryos. D, Alignment of human Mcl1 (isoform 1) and *X. laevis* Mcl1 sequences. In Mcl1 sequence the enriched region in proline (P), glutamic acid (E), serine (S) and threonine (T) residues, referred to as the proline/glutamic acid/serine/threonine (PEST) region is shown in brown. S155, S159 and T163 shown in red are Gsk3 $\beta$  phosphorylation sites either confirmed in human, or putative in *X. laevis*. The *X. laevis* Bcl-2 Homology (BH) domains are shown in blue. In human Mcl1 sequence the black star indicates human S159 and the red star indicates T163. E Overexpression of *flagmcl1* compensates for *Xbax* and *hbak* overexpression. ISH using *sox3* probe was performed at stage 14 *Xenopus* embryos. Four-cell stage embryos were injected in one dorsal blastomere, either with (a) *Xenopus bax (Xbax)*, (b) *Xbax* and *flag-mcl1*, (c) human *bak (hBak)*, and (d) *hbak* and *flag-mcl1* (N=) mRNAs. LacZ mRNA was used as a tracer of the injected side. Embryos are shown dorsal view anterior up. F, Quantification of E. PNE stands for posterior neuroepithelium. White dashed lines indicate the midline. N represents the number of embryos. Relative normalized expression is indicated as means  $\pm$  SE. \*\* $P < .01$ , \*\*\* $P < .001$

Similarly to *flag-mcl1*, overexpression of *Xenopus mcl1 (Xmcl1)* or mouse *mcl1 (mmcl1)*, generated a slight increase in the width of the neuroepithelium

(Figure 6Aa,C). However, the increase was significantly lower compared with that induced by *bcl-XL* overexpression (Figure 6Ad,C) arguing that compared with

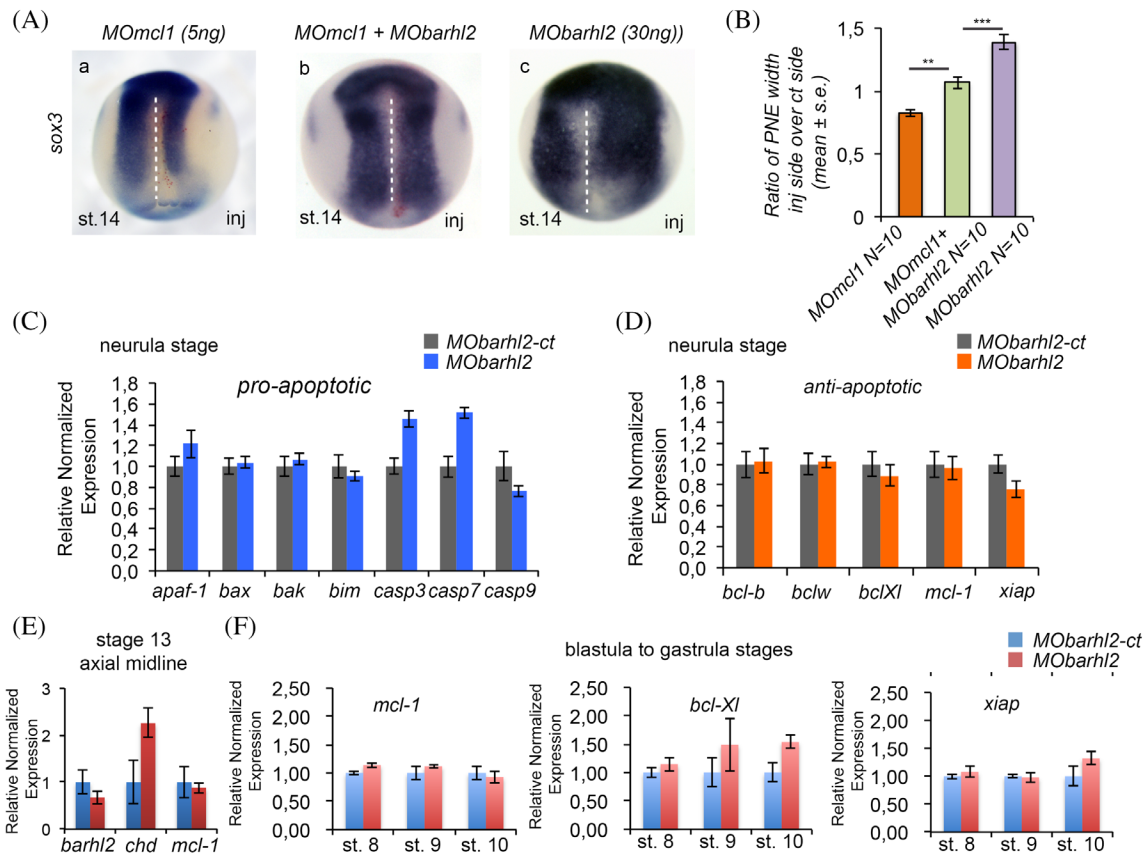


**FIGURE 7** Whereas depletion of the pro-apoptotic transcription factor Barhl2 compensates for Mcl1 depletion, Barhl2 does not regulate *mcl1* transcription, A, Barhl2 depletion rescues Mcl1 depletion. ISH using probes against *sox3* on embryos injected with (a) *MOmcl1* (N = 10); (b) *MOmcl1* and *MObarhl2* (N = 10); (c) *MObarhl2* (N = 10). Representative embryos at stage (st.) 14 are shown dorsal view anterior up. The dashed white line indicates the midline. B, Quantification of A. Relative normalized expression is indicated as means  $\pm$  SE. PNE stands for posterior neuroepithelium. C-F, Analysis of apoptotic genes transcriptional regulation by Barhl2. RT-qPCR analysis on RNA extracted from *X. laevis* individual embryos injected into two dorsal blastomeres at the 2-cell stage either with *MObarhl2-ct* or *MObarhl2*. C,D, st. 13 embryos (N = 10); E, dissected st. 13 axial organizer (N = 10); F, st. 8, 9, and 10 embryos (N = 10). For C-E, expression is normalized relative to Actin and *efl1 $\alpha$* . In F, the expression of *mcl1*, *bcl-xl* and *xiap* is normalized to st. 8. N represents the number of embryos. Relative normalized expression is indicated as means  $\pm$  SEM. *chd* stands for chordin. \*\* $P < .01$ , \*\*\* $P < .001$

*bcl-x<sub>L</sub>*, *mcl1* gain-of-function (GOF) poorly inhibits endogenous apoptosis.

We next asked whether ectopic Mcl1 proteins are degraded within the notochord. Phosphorylation of Mcl1 N-terminal region by kinases such as Gsk3- $\beta$  promotes its phosphorylation and subsequent degradation.<sup>57,58</sup> A comparison of human Mcl1 and *X. laevis* Mcl1 protein sequences indicated a low degree of conservation between the N-terminal parts of human and *Xenopus* Mcl1 (Figure 6D). Despite, putative Gsk3- $\beta$  phosphorylation sites being present in *X. laevis* Mcl1, Serine 159 and Threonine 163, the key residues in Gsk3- $\beta$  mediated downregulation of Mcl1 stability, are conserved (Figure 6D). We investigated the activities of both human *mcl1* (*hmcl1*) and a mutated form of *hmcl1* carrying an Alanine in position 159 instead of a Serine (*hMcl1S159A*). This mutation prevents Gsk3 $\beta$ -mediated phosphorylation of Mcl1 and its subsequent

degradation via the proteasome.<sup>58</sup> Overexpression of both *hmcl1* and *hmcl1S159A* generated the typical enlargement of the neural plate. However, the enlargement of the neural plate was significantly higher in *hmcl1S159A*-injected embryos compared with *hmcl1*-injected ones (Figure 6Abc, C). Of note, the phenotype of *hmcl1S159A* overexpressing embryos is as severe as that of *bcl-x<sub>i</sub>* overexpressing embryos (Figure 6C). We confirmed an increase of the notochord size on the injected side of *hmcl1S159A*-injected embryos (Figure 6B compare a,b). The higher efficiency of a form of Mcl1 resistant to Gsk3- $\beta$ -mediated degradation at inhibiting endogenous apoptosis indicates that Mcl1 protein levels are endogenously regulated within the axial organizer.

We further analyzed the impact of *X.laevis* *bax* (*Xbax*),<sup>55</sup> or human *bak* (*hbak*),<sup>54</sup> overexpression on formation of the axial organizer using *sox3*. Similarly to what was observed upon depletion of Mcl1, *Xbax*, or *hbak*

overexpression induced a diminution of the *sox3* expression territory (Figure 6Ea,c,F) and the coinjection of *Xbax*, or of *hbak*, with *mcl1-flag* significantly reduced the number of embryos exhibiting neuroepithelium size defects (Figure 6Eb-d,F). Therefore Mcl1 overexpression rescues pro-apoptotic factors induced neuroepithelium enlargement phenotype.

These observations argue that Mcl1 protein levels are endogenously regulated within axial organizer cells.

## 2.7 | Depletion of Barhl2 activity compensates for Mcl1 depletion but does not affect apoptotic cascade components' gene expression

Before stage 10, the transcription factor Barhl2 diminishes Spemann organizer fate determination<sup>46</sup>; between stage 10 and stage 14, its overexpression promotes apoptosis in the *Xenopus* dorsal part.<sup>16</sup> We asked whether Barhl2 transcriptionally regulates *mcl1*.

We first investigated whether Barhl2 depletion, which normally increases the notochord size,<sup>16,46</sup> compensates for Mcl1 loss of notochord activity. To inhibit Barhl2 activity, we used a previously characterized MO against Barhl2.<sup>16</sup> The impact of Barhl2 and Mcl1 depletion on formation of the neural plate was analyzed using *sox3*. As previously described, depletion of Mcl1 activity generated a diminution of the *sox3* expression territory (Figure 7Aa, B) whereas *MObarhl2* injected embryos generated a widening of the neural plate (Figure 7Ac,B). Injection of *MOmcl1* together with *MObarhl2* significantly reduced the number of embryos exhibiting neuroepithelium size defects, and the severity of the phenotype (Figure 7Ab,B).

We next asked whether Barhl2 directly or indirectly compensates for Mcl1 ability to inhibit axial organizer cells' decision to die by transcriptional up-regulation of pro-apoptotic genes, or by down-regulation of anti-apoptotic genes. Using Real Time quantitative PCR (RT-qPCR) on the dissected neural plate of stage 13 *MObarhl2-ct* and *MObarhl2* injected individual embryos, we assessed mRNA levels of pro-apoptotic proteins—*apaf-1*, *bax*, *bak*, *bim*, *casp3*, *casp7*, and *casp9*—or anti-apoptotic proteins—*bcl-b*, *bcl-w*, *bcl2l1* encoding *bcl-x<sub>i</sub>*, *mcl1*, and *x-linked inhibitor of apoptosis (xiap)*. In early neurula, *barhl2* depletion does not significantly modify the RNA levels of pro- or anti-apoptotic proteins (Figure 7C,D). Similarly, when RT-qPCR was performed on the dissected axial organizer of stage 13 *MObarhl2-ct* and *MObarhl2* injected embryos, we did not detect any change in *mcl1* RNA levels. In contrast, and in agreement with our previously published results,<sup>16,46</sup> depletion of Barhl2 significantly increases

*chordin* mRNA levels (Figure 7E). As a small peak of *barhl2* transcripts in the presumptive organizer region is detected at stage 8.5 in both *X. tropicalis* and *X. laevis* embryos,<sup>46,50,51</sup> we further quantified the expression changes in the three main anti-apoptotic genes *mcl1*, *xiap*, and *bcl2l1* between stage 8 and stage 10. We did not measure any significant changes in the expression levels of *mcl1*, *bcl-x<sub>i</sub>*, or *xiap*; neither at blastula, nor at early gastrula stages (Figure 7F).

Therefore, whereas Barhl2 depletion compensates for Mcl1 loss-of function between stage 8 and stage 13, it does not affect *mcl1* mRNA levels.

## 3 | DISCUSSION

In this study, performed in *Xenopus* embryos, we confirm a role for the apoptotic machinery in formation of the notochord between late gastrula, early neurula stages. In agreement with Mcl1 expression pattern, Mcl1 activity normally participates in notochord cell survival. Within the notochord cells Mcl1 protein levels are controlled, and a decrease in Mcl1 protein levels initiates the apoptotic program. We also show that Casp7 is the physiological executioner protease in axial organizer cells' apoptosis, whereas Casp3 does not participate to this developmental process.

### 3.1 | Apoptosis in axial organizer development

Our data performed on *Xenopus* embryos, confirm that between late gastrula and early neurula stages PCD is part of neuroepithelium, and more specifically axial organizer, development. In *Xenopus* early neurula, apoptotic nuclei are mostly detected in the dorsal mesoderm and neuroectoderm. A higher rate of dying cells is physiologically and reproducibly observed in a territory bordering the axial organizer and at the border between the ectoderm and the neuroectoderm.<sup>16,35,36</sup> At similar developmental stages, analysis of TUNEL staining in chick and zebrafish support a role for PCD in axial organizer, and ectoderm/neuroectoderm, boundaries formation. In chick, apoptosis is observed in the dorsal midline of the neural plate, at the border between ectoderm and neuroectoderm,<sup>59</sup> in the notochord,<sup>60</sup> and in the floor plate.<sup>14</sup> Finally in zebrafish, TUNEL positive cells are present in the notochord<sup>61</sup> as in *Xenopus* at later developmental stages.<sup>38</sup>

In *Xenopus*, overexpression of human Bcl2, or of *Xenopus* Bcl-X<sub>L</sub>, inhibits apoptosis efficiently,<sup>16,37,39</sup> and induces an enlargement of the neural plate.<sup>16,36</sup> Our

study reveals that the neural plate enlargement is solely detected when Bcl-X<sub>L</sub> is overexpressed in the developing organizer, supporting a role for PCD in sculpting the morphogens' secreting axial midline, including the prechordal plate and the notochord. This "sculpting" activity is similar to that described for apoptosis in limiting the size of the anterior neural ridge, a secondary brain organizing center that secretes Fibroblast growth factor, which patterns the anterior forebrain<sup>15</sup> (reviewed in Reference 4).

Beside a role in controlling axial organizer size, PCD could also be important for correct separation of the notochord from the flanking mesoderm, and/or separation of the floor plate from the neuroectoderm. In the latter case, apoptosis would participate in formation of boundaries between different structures, a role previously reported at later developmental stages (reviewed in References 4, 62).

### 3.2 | Mcl1 physiological activity participates in notochord development

Here we show that in *Xenopus* embryos, at early neurula stages, *mcl1* transcripts are detected in the anterior neural plate, and in the territory flanking the axial organizer. At the same developmental stages, *bcl-xl* transcripts are not detected. Mcl1 expression pattern is congruent with that of TUNEL staining at similar developmental stages. Moreover, Mcl1 depletion decreases notochord cell survival revealing a higher dependence of these cells for Mcl1 anti-apoptotic activities. Mcl1 transcripts are also present at the border between ectoderm and neuroectoderm in agreement with a proposed role for PCD in sharpening the border between neural and non-neural territories.<sup>36,59</sup>

At this date, Mcl1 is the only anti-apoptotic Bcl2 protein that regulates neural progenitor cells survival; and is quite unique, as it is required for the survival of the stem cell niche in the sub-ventricular zone.<sup>63,64</sup> Mice deficient for Mcl1 prematurely die at the peri-implantation stage,<sup>65</sup> which is the most severe phenotype among the anti-apoptotic Bcl-2 proteins. Targeted loss of Mcl1 in neuronal progenitor cells exhibit reduced size of the telencephalon, and atrophied ventricles, with increased apoptosis in neural cells<sup>63</sup> (reviewed in Reference 32. Mcl1 also displays nonapoptotic activities: in mouse neural progenitors it participates in controlling their last mitosis<sup>66</sup> and in *X. laevis* it participates in retinal axon development.<sup>67</sup> Further studies are necessary to determine whether Mcl1 activity in the "sculpting" of organizing centers is conserved in other organizers, and/or between different species. However, our work strengthens the importance of

Mcl1 protein as an anti-apoptotic factor that regulates apoptosis during early developmental steps.

### 3.3 | Mcl1 is endogenously controlled at the post-translational level

Our observations argue that Mcl1 levels are endogenously controlled within the forming axial organizer. Due to the absence of antibody specific for *Xenopus* Mcl1 we could not directly test for Mcl1 protein presence in the neural plate. However, both the similarity of Bax or Bak overexpression phenotypes with that of Mcl1 depletion, and the rescuing of Bax or Bak overexpression phenotype by Mcl1 overexpression strengthen the hypothesis that, similarly to what happens at later developmental stages, the balance between the ratio of pro- vs anti-apoptotic proteins of the Bcl2 family determines whether axial organizer cells live or die. Mcl1 differs from other members of the Bcl-2 family in having a very short half-life.<sup>68</sup> Whereas overexpression of *Xenopus* or of human *mcl1* poorly protects notochord cells from apoptosis, Bcl-X<sub>L</sub> or a form of Mcl1 that cannot be phosphorylated by Gsk3 and subsequently degraded by the proteasome, display a better protective effect indicating that Mcl1 stability is under tight control within the axial organizer cells. Therefore notochord cell death appears to be physiologically triggered by a decrease in Mcl1 protein level.

The regulatory mechanisms of proteasome-mediated degradation of Mcl1 have been well documented for human Mcl1 (reviewed in Reference 69. In human cells, Gsk3- $\beta$  mediated phosphorylation of Mcl1 promotes its interaction with the E3 ubiquitin-ligase  $\beta$ -transducing containing protein ( $\beta$ -TrCP),<sup>57</sup> which catalyzes Mcl1's ubiquitination and subsequent degradation in the proteasome (reviewed in References 32, 69. Beside  $\beta$ -TrCP, the E3 ubiquitin ligase Mcl1 ubiquitin ligase (Mule, also called Huwe1) targets Mcl1 for degradation.<sup>70</sup> Mcl1 is also the target of a deubiquitinase, named Usp9X, which stabilizes Mcl1 by reversing its poly-ubiquitination.<sup>71</sup> Conservation of Gsk3 $\beta$  phosphorylation sites in *Xenopus* Mcl1 suggests that these regulatory roles described in human cells could be conserved in *Xenopus*.

### 3.4 | Casp7 is the executioner protease in early neurula embryos

In both *X. tropicalis* and *X. laevis* a peak of *casp7* transcripts is detected between stage 5 and stage 15.<sup>50,51</sup> MO-mediated depletion of Casp7 generates a dramatic increase in the neuro-epithelium territory, a phenotype similar to that of Bcl-X<sub>L</sub> overexpression. Moreover, the

depletion of Casp7 completely compensates for the decrease in neural plate width induced by a decrease in Mcl1 protein levels. It also efficiently prevents embryos' apoptosis induced by Mcl1 depletion. Our study on stage 10 to stage 14 wild type embryos reveals no correlation between Act-Casp3 positive cells and TUNEL positive cells. Finally, targeted depletion of Casp3 in axial organizer cells has no impact on neural plate development.

Due to their similar proteolytic activities, Casp3 and Casp7 have been suggested to have redundant roles within the apoptotic machinery. A thorough analysis of Casp3 and Casp7 substrates specificities demonstrate that Casp3 is generally more promiscuous, whereas Casp7 proteolysis activities are targeted toward the external cellular machinery supporting a role for this enzyme in separation of tissues during morphogenesis.<sup>72,73</sup> In zebrafish, Caspases inhibitors inhibit early apoptosis.<sup>74</sup> In agreement with our observations, in chick embryos *casp9* expression correlates more closely with TUNEL staining than does *casp3*.<sup>59</sup> Similarly in zebrafish the dynamics of TUNEL staining and *casp3* expression are distinct.<sup>75,76</sup> Mice deficient in *casp7* or in *casp3* genes, as well as mice deficient in both genes indicate some degree of functional compensation between Casp3 and Casp7, as well as distinct activities for these two proteases.<sup>52,77,78</sup> Whereas it remains to be demonstrated whether an early role for Casp7 as the key apoptotic executioner is conserved between species, our data are in agreement with Casp3 and Casp7 exhibiting distinct physiological functions at these early development steps. Indeed in amphibians Casp7 physiologically acts as the executioner enzyme driving axial organizer cells' death, a developmental process occurring independently of Casp3.

The nonproliferative notochord cells originate from the Spemann organizer and both structures are characterized by their ability to secrete the morphogen Shh, anti-BMP, and anti-Wnt, factors. In the drosophila, there are effector's Caspases in the differentiated photoreceptor neurons, which trigger the up-regulation of Hedgehog (Hh) transcription and protein levels.<sup>27,79</sup> Between stage 11 and stage 14 the total number of embryos displaying the characteristic TUNEL positive nuclei pattern in the axial organizer is never more than 5%,<sup>16,36</sup> raising the hypothesis that between stage 11 and stage 14, the local and controlled activation of Casp7 participates in the notochord differentiation process, and maybe in the production of the Shh morphogen. With this view point the activation of Casp7<sup>80</sup> could be part of the notochord cells differentiation program and Mcl1 would play a role in maintaining Casp7 enzymatic activities under strict constrains.

### 3.5 | Despite an evolutionarily conserved activity in regulation of apoptosis, Barhl2 does not act on *mcl1* RNA levels

After stage 8, Barhl2 is expressed in the axial organizer where it switches off the Wnt/ $\beta$ -Catenin-dependent early transcriptional response by a mechanism that depends on histone deacetylase 1 (Hdac-1) activity.<sup>46</sup> In this way Barhl2 pushes Spemann organizer cells toward an irreversible fate commitment. The nonproliferative notochord cells originate from the Spemann organizer, and depletion of the transcription factor Barhl2 increases the size of the axial organizer.<sup>16,46</sup> In coherence with these data, Mcl1 depletion phenotype is compensated for by Barhl2 depletion.

We previously observed that Barhl2 overexpression promotes apoptosis in the *Xenopus* neuroectoderm, and mesoderm.<sup>16,46</sup> A phylogenetic analysis demonstrates that the nematode Ceh-30 is the ortholog of Barhl proteins (reviewed in References 81, 82. Three *C. elegans* genetic screens, performed independently, highlight the regulation of the apoptotic pathway by Barhl orthologs.<sup>43-45</sup> Indeed the sex-specific apoptosis of four cephalic male (CEMs) neurons, which die in hermaphrodites but not males, is under the control of Ceh-30.<sup>44,45</sup> In nematode males, Ceh-30 has been suggested to transcriptionally repress *egl-1*—a BH3-only protein—and *ced-3*—the Caspase-3 ortholog.<sup>43</sup> Between stage 8 and stage 13.5, Barhl2 depletion does not affect *mcl1* mRNA levels and/or transcription of other apoptotic members. These data indicate a more complex mode of apoptosis regulation for Barhl2 in vertebrates (reviewed in Reference 6. It is possible that Barhl2 overexpression induces alterations to Hdac1 activity that are known to cause a genotoxic stress associated with cell cycle arrest and in some cases cell death (reviewed in References 83, 84, but the observations in nematode favor a more specific activity of Barhl2 in regulating the apoptotic machinery which remains to be found.

## 4 | EXPERIMENTAL PROCEDURES

### 4.1 | *Xenopus* embryos care and husbandry

*X. laevis* embryos were obtained by in vitro fertilization and staged using standard procedures.<sup>85,86</sup> Experimental procedures were specifically approved by the ethics committee of both the Institut Curie (Authorization 2016-013 given by CEEA-IC #118) and Institut de Biologie Paris Seine (IBPS) (Authorization 2020-22727 given by CEEA #005) follow the international guidelines (2010/63/UE).

B Durand carries the Authorization for vertebrates' experimental use N75-1548.

## 4.2 | Plasmids

Constructs were generated by sequential PCR amplification followed by subcloning and sequencing in pTOPO (TOPO TA cloning kit Thermofisher) and subcloned in pCS2+. A full-length cDNA for Mcl1 was obtained by RT-PCR (Invitrogen) using stage 14 neural plate *X. laevis* RNA and oligonucleotides 5'-TCATTCTCTCCCTGCTGCTGAGAG AC-3' and 5'-TCATCGGATCATGTACGCCAAACCGG-3' using information from Xenbase (<http://www.xenbase.org/>, RRID:SCR\_003280). Mcl1 full-length cDNA was subcloned in pCS2+. The tagged constructs were generated by subcloning in either pCS2-Myc (C-terminal Myc tag for Mcl1-Myc), or pCS2+Flag (N-terminal Flag for Flag-Mcl1). pTOPO-Mcl1 was a gift from Ulrich Maurer (Addgene plasmid #21605). PTOPO-Mcl1S159A was a gift from Ulrich Maurer (Addgene plasmid #21606). *Xenopus bax* in pCS2 was a gift from L. Sachs.<sup>55</sup> EGFP-Bak pcDNA1 was a gift from Richard Youle (Addgene plasmid # 32564; <http://n2t.net/addgene:32564>; RRID:Addgene\_32564). The sequence of all plasmids is available upon request.

## 4.3 | mRNA synthesis, antisense morpholinos, and injections

Synthetic capped RNAs were prepared from pCS2+ derivatives with mMessage mMachine kit (Ambion). Antisense MO either with no 5' capping, either coupled to fluorescein were made by Gene-Tools as previously published: *MObarhl2*<sup>16</sup> (30 ng), *MOcasp3*<sup>49</sup> (40 ng), *MOmcl1-1* (5 ng), *MOmcl1-2* (10 ng), *MOmcl1-ct* (10 ng) *MOcasp7* (12 ng), and control MO (*MOct*) (20 ng). Sequences of MO are given in Table 1. MO were diluted in RNase free water at 1 nmol/μl, kept at -80°C and heated 10 min at 65°C before use. Except when otherwise specified, MOs or mRNAs were co-injected with β-gal mRNA (100 pg) or *gfp* mRNA (100 pg) or *MOct* coupled to fluorescein for lineage tracing (3 ng). β-gal activity was revealed in Red-Gal (Research Organics) staining solution. Embryos were injected unilaterally for ISH/morphology and on both sides for WB and RT-qPCR. Three independent experiments were performed and the results were pooled. For all rescue experiments, we selected the minimal mRNA quantity that both induced the specific phenotype and displayed no toxicity. Except when indicated otherwise, after stage 10 the embryos are shown dorsal view, anterior up. At stage 10 and below, embryos are shown ventral view dorsal

up. For rescue experiments the means between different data sets were compared using the Wilcoxon signed-rank test and significant differences are indicated with asterisks (see Section 4.10).

## 4.4 | Reverse transcription polymerase chain reaction (RT-PCR)

Total RNA from embryos was extracted using the Qiagen RNeasy Kit. RT-PCR analysis was carried out with the Superscript One-step Kit (Invitrogen) using specific primers resumed in Table 2. Histone 4 was used as a loading control and water was used as a negative control.

## 4.5 | Quantitative reverse transcription polymerase chain reaction (RT-qPCR)

For each time point RNA extract was obtained at least twice from five individual embryos obtained from the same fertilization. Embryos were dissociated by pipetting up-and-down with a 26G needle in Trizol (Invitrogen) and extracted according to manufacturer instructions. The RNA pellet was suspended in RNase free water and kept at -80°C. RNA samples were reverse-transcribed using MMLV-RT enzyme (Promega). RT-qPCR was carried out using IQ SYBR green Supermix (BioRad) on a CFX96 touch Real-Time PCR Detection System (BioRad). RT-qPCRs were performed on embryos using standard procedures (39 cycles) using technical triplicates for each time point. Primers were designed using Primer 3 (<http://www.bioinformatics.nl/cgi-bin/primer3plus/primer3plus.cgi/>). Primers were selected based on their amplification efficiency and specificity. *Elongation factor 1 (ef1)* and *ornithine decarboxylase (odc)* primers were used as controls. Primers oligomers used in RT-qPCR are resumed in Table 3.

## 4.6 | TUNEL staining

Whole-mount TUNEL staining was performed as previously described, except embryos were not pretreated in hydroxyurea.<sup>36,89</sup>

## 4.7 | Immunostaining against Act-Casp3

Immunostaining was performed using a rabbit polyclonal anti-Cleaved Casp3 antibody, as described previously<sup>90</sup> (Table 3). The anti-Cleaved Casp3 antibody was detected using anti-rabbit (Ig) antibodies conjugated to alkaline

Gene	Morpholino sequence	Dose (ng)	Reference
<i>mcl1-ct</i>	AACCAGTAAGTCCCTTTCACCCAGA	20	This study
<i>mcl1-1</i>	GCGCCTAATCCTAAAGACCTTGTGT	10	This study
<i>mcl1-2</i>	AAGCACTAACTCCGTTTCACGCAGA	10	This study
<i>casp7</i>	TCATTGTGGTCTTGCTGAGCCAC	12	This study
<i>Moct</i>	CCTCTTACCTCAGTTACAATTTATA	20	Gene-tools
<i>casp3</i>	ACCATTCTGGGATTCTCCATcttg	40	87

**TABLE 1** Morpholinos used in this study

**TABLE 2** Primers used for RT-PCR in this study

Gene	Forward	Reverse	Reference
<i>histone 4</i>	ATGTCCGGCCCGGGCAAAGG	AGCCGTAGAGAGTGCGGCC	This study
<i>Casp7</i>	GCTGCTTCAAGGGCCTCGGC	GGCTCAGGAATATGCAGGCG	This study

**TABLE 3** Primers used for RT-qPCR in this study

Gene	Forward	Reverse	Reference
<i>apaf-1</i>	TGCTTCACGAGGGGTACAAA	CTCCCTCACAGAGTACGGTT	This study
<i>bak</i>	TAATTGGAAGAATGCCGCC	GAATGGGCAGCGAGGATTTT	This study
<i>bax</i>	GAATGGGCAGCGAGGATTTT	TAATTGGAAGAATGCCGCC	This study
<i>bcl2l10</i>	GGACTGGCTGCAGAGTAGC	TGCCCGCTGAGTCCTCT	This study
<i>bcl-xl</i>	TGTGGAGAGTGCAAACAAGG	ACAGGCCAACAAAAGCTTCC	This study
<i>Bcl2l2</i>	TGAGAGGCTGGATTCAGAGC	GCCTCCTGGCTTCTTCTATGG	This study
<i>bcl-2</i>	GACAGATCTCAGGGCTCCTC	CCTTCCCCAGTTTACCCAT	This study
<i>bim</i>	GGAGGAGCAGCGATGAAGAA	TTGTAACTGGCCACCTTCAC	This study
<i>casp3</i>	AGAGGAGACCGATGCAAGAC	CTCCACTGGAATACGCTGGA	This study
<i>casp7</i>	ACTGACCACTCTTCCCGTG	ATCTGCCTCCAACCCATCAT	This study
<i>caspase-9</i>	ATGCCACCCCTGTTTTCTCT	ATCCCTCCATGACACGTAGC	This study
<i>efl</i>	ACACTGCTCACATTGCTTGC	AGAAGCTCTCCACGCACATT	This study
<i>mcl1</i>	CCTTCACGGGCATGCTACA	AGCGGGAACCTCAGAAAGTTT	This study
<i>odc</i>	CATGGCATTCTCCCTGAAGT	TGGTCCCAAGGCTAAAGTTG	88
<i>xiap</i>	TCACCTGCATTACCCAAGGA	ATCCGCACATACAGCACATG	This study

phosphatase (Roche), followed by a staining using 4-Nitro blue tetrazolium chloride (NBT)/5-bromo-4-chloro-3-indoyl-phosphate (BCIP) substrates (Roche). The primary antibody and folds of dilutions of each antibody used for the detection of tagged or endogenous proteins are described in Tables 4 and 5.

#### 4.8 | Whole mount ISH and Paraffin sectioning

Control or injected embryos were collected at indicated stages. ISH were performed using digoxigenin labeled probes. Antisense probes were generated for *Xenopus*

*mcl1*, *bcl-Xl*, *sox3*, and *EpKer* according to the manufacturer's instructions (RNA Labeling Mix, Roche). ISH was processed following protocol described previously.<sup>87</sup> Briefly, following overnight incubation with the probes and then with alkaline Phosphatase-conjugated anti-DIG enzymatic activity was revealed using NBT/BCIP substrates (Roche). Then, bleaching treatment was performed after the postfixation of the embryos. Whole mount images were captured using stereomicroscope Lumar V12. Sections (40  $\mu$ m thickness) were cut using a Leica VT1000 vibratome after gelatin-albumin embedding. Pictures were captured using a digital Axiocam 506 color camera on a Zeiss microscope on PICT-IBiSA@Orsay Histology facility of Institut Curie and

**TABLE 4** Primary antibodies used in this study

Primary antibody	Source	Host	Dilution
Actin	Sigma-Aldrich A2066	Rabbit	1:2000 (WB)
c-Myc epitope	SC clone 9E10	Mouse	1:5000 (WB)
Flag epitope	Sigma-Aldrich F7425	Rabbit	1:1000 (WB)
Cleaved Casp3	Cell Signaling 9661	Rabbit	1:500 (IHC)

Abbreviations: IHC, Immunohistochemistry; WB, western blot.

**TABLE 5** Secondary antibodies used in this study

Secondary antibody	Source	Host	Dilution
HCP anti-mouse IgG	Jackson Immuno Research 115-035-003	Goat	1:10 000 (WB)
HCP anti-rabbit IgG	Jackson Immuno Research 111-035-003	Goat	1:10 000 (WB)
Alkaline phosphatase anti-rabbit IgG	Roche A3687	Goat	1:500 (IHC)

Abbreviations: IHC, Immunohistochemistry; WB, western blot.

processed with Zen program (version2.3), ImageJ, and Adobe Photoshop CS6 software. For paraffin sections the embryos were kept long term in ethanol 100% then incubated in butanol 100% over night. The embryos were bathed successively in paraffin (Paraplast Plus, Sigma) then processed for microtome section at 20  $\mu$ m (Leica, RM2125 RTS). Sections were unwrapped by three Xylene baths and mounted in EUKITT.

#### 4.9 | Protein extraction and WB

Embryos were lysed on ice in lysis buffer containing 1% Triton x-100, 5 mM EDTA, 5 mM EGTA, 50 mM Tris pH 7.5, 0.3 M NaCl, 1 $\times$  complete proteases inhibitor (Roche 11697498001) and 1 $\times$  PhosSTOP phosphatase inhibitor (Roche 04906837001). Whole cell lysates were cleared via centrifugation at 14 000g for 30 min. Protein quantification was performed using the BioRad Pc Protein Assay (BioRad). Samples were denatured with 1/2 volume of 2 $\times$  Laemli Buffer (BioRad) and  $\beta$ -mercaptoethanol and boiled for 5 min. Twenty micro gram of protein extracts were separated by a 10% or 12% SDS-polyacrylamide gel and then transferred to a PVDF membrane (Immobilon-P, Millipore).

Blots were blocked with 5% milk and were detected with an ECL Western Blotting Detection Reagent (Amersham RPN2109). Densitometry analysis, standardized to actin as a control for protein loading, was performed using the ImageJ software. The primary antibodies and folds of dilutions of each antibody used for the detection of tagged or endogenous proteins are described in Tables 4 and 5.

#### 4.10 | Statistical analysis and sequence alignment

For all rescue experiments the means between different data sets were compared using the Wilcoxon signed-rank test. All statistical analyses were performed using Real statistics plugin from Microsoft Excel. N stands for the number of embryos. Significant differences are indicated with asterisks: \**P*-value  $\leq .05$ ; \*\* *P*-value  $\leq .01$ ; \*\*\**P*-value  $\leq .001$ . The alignment of human Mcl1 (isoform 1) and *X. laevis* Mcl1 sequences was done using the Needleman-Wunsch Global Align Nucleotide Sequences (<https://blast.ncbi.nlm.nih.gov/>).

#### ACKNOWLEDGMENTS

The authors greatly acknowledge the PICT-IBISA@Orsay, Histology and Imaging Facilities, of the Institut Curie supported by the French National Research Agency through the “Investments for the Future” program (Fran-BioImaging, ANR-10-INSB-04), the “Plateau Technique de Biologie Moléculaire” of I2BC (Véronique Henriot) for construction of plasmids and Elodie Belloir, Virginie Dangles and Isabelle Grandjean for animal care. We also acknowledge Simon Saule for help and advice, and Paul Johnson and Emma Dumble for their editing work on the manuscript. This work was supported by the Centre National de la Recherche Scientifique (CNRS—UMR3347), the Institut National de la Santé Et de la Recherche Médicale (INSERM—U1021) l’Institut Curie (ETIC), and donors to B Durand project, l’Université Paris-Sud, the Fondation Pierre Gilles de Gennes (FPGG0039), and the Ligue Nationale contre le Cancer Comité Ile de France (RS19/75-52). The Centre National de la Recherche Scientifique supports Béatrice Durand. Elena Sena is supported by a fellowship from the “Ministère de la Recherche” and “Association pour la Recherche sur le Cancer”(DOC20170505923). J. Bou-Rouphael is supported by a fellowship from the “Ministère de la Recherche”. Sorbonne Université supports Clémence Carron-Homo.

#### AUTHOR CONTRIBUTIONS

**Elena Sena:** Conceptualization; data curation; formal analysis; investigation; methodology; resources;

validation; writing-original draft. **Johnny Bou-Rouphael**: Data curation; formal analysis; investigation; methodology; resources; validation. **Nathalie Rocques**: Conceptualization; data curation; formal analysis; investigation; methodology; resources; validation. **Clemence Carron**: Investigation; methodology; resources.

## ORCID

Elena Sena  <https://orcid.org/0000-0003-1220-5639>

Béatrice C. Durand  <https://orcid.org/0000-0002-0047-288X>

## REFERENCES

- Kerr JF, Harmon B, Searle J. An electron-microscope study of cell deletion in the anuran tadpole tail during spontaneous metamorphosis with special reference to apoptosis of striated muscle fibers. *J Cell Sci.* 1974;14:571-585.
- Kerr JF. History of the events leading to the formulation of the apoptosis concept. *Toxicology.* 2002;181-182:471-474.
- Arya R, White K. Review: cell death in development: signaling pathways and core mechanisms. *Seminars in Cell and Developmental Biology.* 2015;39:12-19.
- Yamaguchi Y, Miura M. Programmed cell death in neurodevelopment. *Dev Cell.* 2015;32:478-490.
- de la Rosa EJ, de Pablo F. Cell death in early neural development: beyond the neurotrophic theory. *Trends Neurosci.* 2000;23:454-458.
- Juraver-Geslin HA, Durand BC. Early development of the neural plate: new roles for apoptosis and for one of its main effectors caspase-3. *Genesis.* 2015;53:203-224.
- Kuan CY, Roth KA, Flavell RA, Rakic P. Mechanisms of programmed cell death in the developing brain. *Trends Neurosci.* 2000;23:291-297.
- Yeo W, Gautier J. Early neural cell death: dying to become neurons. *Dev Biol.* 2004;274:233-244.
- Anderson C, Stern CD. Organizers in Development. *Curr Top Dev Biol.* 2016;117:435-454.
- Carron C, Shi DL. Specification of anteroposterior axis by combinatorial signaling during *Xenopus* development. *Wiley Interdiscip Rev Dev Biol.* 2016;5:150-168.
- Kiecker C, Lumsden A. The role of organizers in patterning the nervous system. *Annu Rev Neurosci.* 2012;35:347-367.
- Sena E, Feistel K, Durand BC. An evolutionarily conserved network mediates development of the zona limitans intrathalamica, a sonic hedgehog-secreting caudal forebrain Signaling Center. *J Dev Biol.* 2016;4:31.
- Agarwala S, Sanders TA, Ragsdale CW. Sonic hedgehog control of size and shape in midbrain pattern formation. *Science.* 2001;291:2147-2150.
- Homma S, Yaginuma H, Oppenheim RW. Programmed cell death during the earliest stages of spinal cord development in the chick embryo: a possible means of early phenotypic selection. *J Comp Neurol.* 1994;345:377-395.
- Nonomura K, Yamaguchi Y, Hamachi M, et al. Local apoptosis modulates early mammalian brain development through the elimination of morphogen-producing cells. *Dev Cell.* 2013;27:621-634.
- Offner N, Duval N, Jamrich M, Durand B. The pro-apoptotic activity of a vertebrate Bar-like homeobox gene plays a key role in patterning the *Xenopus* neural plate by limiting the number of chordin- and shh-expressing cells. *Development.* 2005;132:1807-1818.
- Yeo W, Gautier J. XNGNR1-dependent neurogenesis mediates early neural cell death. *Mech Dev.* 2005;122:635-644.
- Ellis HM, Horvitz HR. Genetic control of programmed cell death in the nematode *C. elegans*. *Cell.* 1986;44:817-829.
- Fuchs Y, Steller H. Programmed cell death in animal development and disease. *Cell.* 2011;147:742-758.
- Hyman BT, Yuan J. Apoptotic and non-apoptotic roles of caspases in neuronal physiology and pathophysiology. *Nat Rev Neurosci.* 2012;13:395-406.
- Yi CH, Yuan J. The Jekyll and Hyde functions of caspases. *Dev Cell.* 2009;16:21-34.
- Lamkanfi M, Festjens N, Declercq W, Vanden Berghe T, Vandennebee P. Caspases in cell survival, proliferation and differentiation. *Cell Death Differ.* 2007;14:44-55.
- Oppenheim RW, Flavell RA, Vinsant S, Prevette D, Kuan CY, Rakic P. Programmed cell death of developing mammalian neurons after genetic deletion of caspases. *J Neurosci.* 2001;21:4752-4760.
- Zheng TS, Flavell RA. Divinations and surprises: genetic analysis of caspase function in mice. *Exp Cell Res.* 2000;256:67-73.
- Weil M, Jacobson MD, Raff MC. Are caspases involved in the death of cells with a transcriptionally inactive nucleus? Sperm and chicken erythrocytes. *J Cell Sci.* 1998;111(Pt 18):2707-2715.
- Weil M, Raff MC, Braga VM. Caspase activation in the terminal differentiation of human epidermal keratinocytes. *Curr Biol.* 1999;9:361-364.
- Fan Y, Bergmann A. Apoptosis-induced compensatory proliferation. The cell is dead. Long live the cell! *Trends Cell Biol.* 2008a;18:467-473.
- Perez-Garijo A, Steller H. Spreading the word: non-autonomous effects of apoptosis during development, regeneration and disease. *Development.* 2015;142:3253-3262.
- Tsuchiya Y, Murai S, Yamashita S. Apoptosis-inhibiting activities of BIR family proteins in *Xenopus* egg extracts. *FEBS J.* 2005;272:2237-2250.
- Tsuchiya Y, Yamashita S. Anti-apoptotic activity and proteasome-mediated degradation of *Xenopus* Mcl-1 protein in egg extracts. *J Biol Chem.* 2011;286:15806-15814.
- Happo L, Strasser A, Cory S. BH3-only proteins in apoptosis at a glance. *J Cell Sci.* 2012;125:1081-1087.
- Opferman JT, Kothari A. Anti-apoptotic BCL-2 family members in development. *Cell Death Differ.* 2018;25:37-45.
- Raff M. Cell suicide for beginners. *Nature.* 1998;396:119-122.
- Raff MC. Social controls on cell survival and cell death. *Nature.* 1992;356:397-400.
- Hensey C, Gautier J. Programmed cell death during *Xenopus* development: a spatio-temporal analysis. *Dev Biol.* 1998;203:36-48.
- Yeo W, Gautier J. A role for programmed cell death during early neurogenesis in *xenopus*. *Dev Biol.* 2003;260:31-45.
- Johnston J, Chan R, Calderon-Segura M, McFarlane S, Browder LW. The roles of Bcl-xL in modulating apoptosis during development of *Xenopus laevis*. *BMC Dev Biol.* 2005;5:20.
- Malikova MA, Van Stry M, Symes K. Apoptosis regulates notochord development in *Xenopus*. *Dev Biol.* 2007;311:434-448.

39. Van Stry M, McLaughlin KA, Ataliotis P, Symes K. The mitochondrial-apoptotic pathway is triggered in *Xenopus* mesoderm cells deprived of PDGF receptor signaling during gastrulation. *Dev Biol.* 2004;268:232-242.
40. Nehme R, Conradt B. Egl-1: a key activator of apoptotic cell death in *C. elegans*. *Oncogene.* 2008;27(1):S30-S40.
41. Li S, Price SM, Cahill H, Ryugo DK, Shen MM, Xiang M. Hearing loss caused by progressive degeneration of cochlear hair cells in mice deficient for the *Barhl1* homeobox gene. *Development.* 2002;129:3523-3532.
42. Li S, Qiu F, Xu A, Price SM, Xiang M. *Barhl1* regulates migration and survival of cerebellar granule cells by controlling expression of the neurotrophin-3 gene. *J Neurosci.* 2004;24:3104-3114.
43. Nehme R, Grote P, Tomasi T, et al. Transcriptional upregulation of both *egl-1* BH3-only and *ced-3* caspase is required for the death of the male-specific CEM neurons. *Cell Death Differ.* 2010;17:1266-1276.
44. Peden E, Kimberly E, Gengyo-Ando K, Mitani S, Xue D. Control of sex-specific apoptosis in *C. elegans* by the *BarH* homeodomain protein CEH-30 and the transcriptional repressor UNC-37/Groucho. *Genes Dev.* 2007;21:3195-3207.
45. Schwartz HT, Horvitz HR. The *C. elegans* protein CEH-30 protects male-specific neurons from apoptosis independently of the *Bcl-2* homolog *CED-9*. *Genes Dev.* 2007;21:3181-3194.
46. Sena E, Rocques N, Borday C, et al. *Barhl2* maintains T cell factors as repressors and thereby switches off the Wnt/beta-Catenin response driving Spemann organizer formation. *Development.* 2019;146:dev173112.
47. Gavrieli Y, Sherman Y, Ben-Sasson SA. Identification of programmed cell death in situ via specific labeling of nuclear DNA fragmentation. *J Cell Biol.* 1992;119:493-501.
48. Srinivasan A, Roth KA, Sayers RO, et al. In situ immunodetection of activated caspase-3 in apoptotic neurons in the developing nervous system. *Cell Death Differ.* 1998;5:1004-1016.
49. Juraver-Geslin HA, Ausseil JJ, Wassef M, Durand BC. *Barhl2* limits growth of the diencephalic primordium through Caspase3 inhibition of beta-catenin activation. *Proc Natl Acad Sci U S A.* 2011;108:2288-2293.
50. Owens ND, Blitz IL, Lane MA, et al. Measuring absolute RNA copy numbers at high temporal resolution reveals transcriptome kinetics in development. *Cell Rep.* 2016;14:632-647.
51. Session AM, Uno Y, Kwon T, et al. Genome evolution in the allotetraploid frog *Xenopus laevis*. *Nature.* 2016;538:336-343.
52. Houde C, Banks KG, Coulombe N, et al. Caspase-7 expanded function and intrinsic expression level underlies strain-specific brain phenotype of caspase-3-null mice. *J Neurosci.* 2004;24:9977-9984.
53. Ruchaud S, Korfali N, Villa P, et al. Caspase-6 gene disruption reveals a requirement for lamin A cleavage in apoptotic chromatin condensation. *EMBO J.* 2002;21:1967-1977.
54. Nechushtan A, Smith CL, Lamensdorf I, Yoon SH, Youle RJ. Bax and Bak coalesce into novel mitochondria-associated clusters during apoptosis. *J Cell Biol.* 2001;153:1265-1276.
55. Sachs LM, Abdallah B, Hassan A, et al. Apoptosis in *Xenopus* tadpole tail muscles involves Bax-dependent pathways. *FASEB J.* 1997;11:801-808.
56. Brenner D, Mak TW. Mitochondrial cell death effectors. *Curr Opin Cell Biol.* 2009;21:871-877.
57. Ding Q, He X, Hsu JM, et al. Degradation of Mcl-1 by beta-TrCP mediates glycogen synthase kinase 3-induced tumor suppression and chemosensitization. *Mol Cell Biol.* 2007;27:4006-4017.
58. Maurer U, Charvet C, Wagman AS, Dejardin E, Green DR. Glycogen synthase kinase-3 regulates mitochondrial outer membrane permeabilization and apoptosis by destabilization of MCL-1. *Mol Cell.* 2006;21:749-760.
59. Gibson A, Robinson N, Streit A, Sheng G, Stern CD. Regulation of programmed cell death during neural induction in the chick embryo. *Int J Dev Biol.* 2011;55:33-43.
60. Hirata M, Hall BK. Temporospatial patterns of apoptosis in chick embryos during the morphogenetic period of development. *Int J Dev Biol.* 2000;44:757-768.
61. Cole LK, Ross LS. Apoptosis in the developing zebrafish embryo. *Dev Biol.* 2001;240:123-142.
62. Jacobson MD, Weil M, Raff MC. Programmed cell death in animal development. *Cell.* 1997;88:347-354.
63. Arbour N, Vanderluit JL, Le Grand JN, et al. Mcl-1 is a key regulator of apoptosis during CNS development and after DNA damage. *J Neurosci.* 2008;28:6068-6078.
64. Malone CD, Hasan SM, Roome RB, et al. Mcl-1 regulates the survival of adult neural precursor cells. *Mol Cell Neurosci.* 2012;49:439-447.
65. Rinckenberger JL, Horning S, Klocke B, Roth K, Korsmeyer SJ. Mcl-1 deficiency results in peri-implantation embryonic lethality. *Genes Dev.* 2000;14:23-27.
66. Hasan SM, Sheen AD, Power AM, et al. Mcl1 regulates the terminal mitosis of neural precursor cells in the mammalian brain through p27Kip1. *Development.* 2013;140:3118-3127.
67. Roque CG, Wong HH, Lin JQ, Holt CE. Tumor protein Tctp regulates axon development in the embryonic visual system. *Development.* 2016;143:1134-1148.
68. Okamoto T, Coultas L, Metcalf D, et al. Enhanced stability of Mcl1, a prosurvival Bcl2 relative, blunts stress-induced apoptosis, causes male sterility, and promotes tumorigenesis. *Proc Natl Acad Sci U S A.* 2014;111:261-266.
69. Thomas LW, Lam C, Edwards SW. Mcl-1; the molecular regulation of protein function. *FEBS Lett.* 2010;584:2981-2989.
70. Zhong Q, Gao W, Du F, Wang X. Mule/ARF-BP1, a BH3-only E3 ubiquitin ligase, catalyzes the polyubiquitination of Mcl-1 and regulates apoptosis. *Cell.* 2005;121:1085-1095.
71. Schwickart M, Huang X, Lill JR, et al. Deubiquitinase USP9X stabilizes MCL1 and promotes tumour cell survival. *Nature.* 2010;463:103-107.
72. Brentnall M, Rodriguez-Menocal L, De Guevara RL, Cepero E, Boise LH. Caspase-9, caspase-3 and caspase-7 have distinct roles during intrinsic apoptosis. *BMC Cell Biol.* 2013;14:32.
73. Walsh JG, Cullen SP, Sheridan C, Luthi AU, Gerner C, Martin SJ. Executioner caspase-3 and caspase-7 are functionally distinct proteases. *Proc Natl Acad Sci U S A.* 2008;105:12815-12819.
74. Negron JF, Lockshin RA. Activation of apoptosis and caspase-3 in zebrafish early gastrulae. *Dev Dyn.* 2004;231:161-170.
75. Ikegami R, Hunter P, Yager TD. Developmental activation of the capability to undergo checkpoint-induced apoptosis in the early zebrafish embryo. *Dev Biol.* 1999;209:409-433.
76. Yabu T, Kishi S, Okazaki T, Yamashita M. Characterization of zebrafish caspase-3 and induction of apoptosis through

- ceramide generation in fish fathead minnow tailbud cells and zebrafish embryo. *Biochem J.* 2001;360:39-47.
77. Kuida K, Zheng TS, Na S, et al. Decreased apoptosis in the brain and premature lethality in CPP32-deficient mice. *Nature.* 1996;384:368-372.
78. Lakhani SA, Masud A, Kuida K, et al. Caspases 3 and 7: key mediators of mitochondrial events of apoptosis. *Science.* 2006;311:847-851.
79. Fan Y, Bergmann A. Distinct mechanisms of apoptosis-induced compensatory proliferation in proliferating and differentiating tissues in the *Drosophila* eye. *Dev Cell.* 2008b;14:399-410.
80. Mille F, Thibert C, Fombonne J, et al. The Patched dependence receptor triggers apoptosis through a DRAL-caspase-9 complex. *Nat Cell Biol.* 2009;11:739-746.
81. Reig G, Cabrejos ME, Concha ML. Functions of BarH transcription factors during embryonic development. *Dev Biol.* 2007;302:367-375.
82. Schuhmacher LN, Albadri S, Ramialison M, Poggi L. Evolutionary relationships and diversification of barhl genes within retinal cell lineages. *BMC Evol Biol.* 2011;11:340.
83. Coates PJ, Lorimore SA, Wright EG. Cell and tissue responses to genotoxic stress. *J Pathol.* 2005;205:221-235.
84. Zhang J, Zhong Q. Histone deacetylase inhibitors and cell death. *Cell Mol Life Sci.* 2014;71:3885-3901.
85. Nieuwkoop PD, Faber J. In: Nieuwkoop PD, Faber J, eds. *Normal table of *Xenopus laevis* (Daudin): a systematical and chronological survey of the development from the fertilized egg till the end of metamorphosis.* New York, NY: Garland Publishing; with a foreword by John Gerhart and Marc Kirschner; 1994, 1994.
86. Sive HL, Grainger RM, Harland RM. In: Sive HL, Grainger RM, Harland RM, eds. *Early development of *Xenopus laevis*: a laboratory manual.* Cold Spring Harbor, NY: Cold Spring Harbor Laboratory Press; 2000:c2000.
87. Juraver-Geslin HA, Gomez-Skarmeta JL, Durand BC. The conserved barH-like homeobox-2 gene barhl2 acts downstream of orthodenticle-2 and together with iroquois-3 in establishment of the caudal forebrain signaling center induced by Sonic Hedgehog. *Dev Biol.* 2014;396:107-120.
88. Milet C, Maczkowiak F, Roche DD, Monsoro-Burq AH. Pax3 and Zic1 drive induction and differentiation of multi potent, migratory, and functional neural crest in *Xenopus* embryos. *Proc Natl Acad Sci.* 2013;110:5528-5533.
89. Hensey C, Gautier J. A developmental timer that regulates apoptosis at the onset of gastrulation. *Mech Dev.* 1997;69:183-195.
90. Saka Y, Smith JC. Spatial and temporal patterns of cell division during early *Xenopus* embryogenesis. *Dev Biol.* 2001;229:307-318.

**How to cite this article:** Sena E, Bou-Rouphael J, Rocques N, Carron-Homo C, Durand BC. Mcl1 protein levels and Caspase-7 executioner protease control axial organizer cells survival. *Developmental Dynamics.* 2020;1–20. <https://doi.org/10.1002/dvdy.169>